University of Twente
Department of Mechanical Engineering

Determination of the transverse stress in a combined tensile–shear test

M. van Riel

Master's thesis

February 2005

Exam committee:

Supervisor:	Prof. dr. ir. J. Huétink
Mentor:	Dr. ir. A.H. van den Boogaard
Second Mentor:	Dr. ir. C.H.L.J. ten Horn
External Member:	Dr. ir. T.C. Bor

Exam date:	23th of February 2005
Report number:	CTW.05/TM-5496

Summary

In this thesis the possiblities to determine the complete stress state with the *biaxial tester* are investigated. The test equipment can load a specimen of sheet material with both shear and tensile force. This research is done because the possiblities of the *biaxial tester* which are intuitively available, are not used.

The specimen used in the *biaxial tester* has a large width-to-height ratio, which results in a transverse stress in the specimen during loading. The forces in tensile and shear direction are easily measured and the stresses in shear and tensile direction are simply calculated. The full description, however, can not be determined because the transverse stress is unknown. This is a result of the constraint, imposed by the large width-to-height ratio. The strains are directly measured on the surface. By imposing the *principle of normality*, the tangent of the yield surface is known and the transverse stress can be calculated.

To test the algorithm, different simulations are performed. These are performed in DIEKA for a relatively smooth yield locus and a strongly curved yield locus. Proved is that the concept works. The results however depend heavily on the strain increments during the test. Tensile strain increments of $2 \cdot 10^{-6}$ give results which are within 1 % error of the 'exact' solution. Larger increments result in a larger deviation.

The algorithm is not yet usable on the *biaxial tester*. The required accuracy for the algorithm are too high for the *biaxial tester* to satisfy.

Samenvatting

In dit afstudeerverslag worden de mogelijkheden om de complete spanningstoestand te bepalen met de *biaxiale testbank* onderzocht. Deze testopstelling belast plaatmateriaal op zowel afschuiving als op een normaalspanning. Dit onderzoek is gedaan omdat de mogelijkheden van de *biaxiale testbank*, die intïutief wel aanwezig zijn, niet ten volle benut worden.

De testplaatjes die gebruikt worden in de *biaxiale testbank* hebben een grote breedte-hoogte verhouding, wat resulteert in een dwars-spanning gedurende de test. De normaal- en schuif-krachten zijn eenvoudig te meten met de opstelling en zijn tevens makkelijk om te rekenen naar spanningen. De volledige beschrijving van de spanningstoestand kan echter niet bepaald worden omdat de dwars-spanning niet bekend is. Dit is een gevolg van de restrictie opgelegd door de breedt-hoogte verhouding. De rekken zijn wel direct te meten, rechtstreeks van het oppervlak. Door aan te nemen dat het materiaal zich gedraagt naar het *normaliteitsprincipe*, de tangent van het vloeioppervlak is bekend en de dwarsspaning kan berekend worden.

Om het algoritme te testen zijn verschillende simulaties uitgevoerd. Deze zijn alle uitgevoerd in DIEKA, voor zowel vloeioppervlakken met een glad verloop als met een knik in het oppervlak. Aangetoond is dat het concept werkt. Echter, de resultaten zijn sterk afhankelijk van de grootte van de rekincrementen die gebruikt worden in de simulaties. Verticale rek incrementen van $2 \cdot 10^{-6}$ geven resultaten die binnen 1% van de 'exacte' oplossingen liggen. Grotere incrementen geven een grotere afwijking.

Het algoritme is nog niet toepasbaar. Het algoritme heeft een nauwkeurigheid nodig van de gegevens, waar de *biaxiale testbank* nog niet aan kan voldoen.

Contents

Chapter 1

Introduction

1.1 Background

These days metal is still the most used material to produce various types of products. For relatively large constructions such as drilling rigs but also the smallest as watches. One part of the metal industry is sheet metal forming industry. This engages in among others, the automotive industry and the packaging industry. This thesis is within this framework of sheet metal forming.

For the most engineering processes some kind of force field in the specifications is present. For instance, in the automotive industry one of the targets in designing a new car is to make it lighter than its predecessor. On the other hand, the specifications on stiffness are increased. To choose the right design asks for detailed information on the used materials.

The processes that take place within the sheet material are well described with all sort of simulation programmes. The software keeps getting better, and also the description of the behaviour of the metal when it is produced is accurately predicted. This is of great importance for crash tests with cars, for instance. The programs used are without exception FEM, Finite Element Method.

A way to characterise materials is by their yield limit, at which point the stress reaches a level at which the deformation becomes plastic instead of elastic. For sheet material, which is two dimensional, a yield surface can be recognised. The accuracy of the description of this yield surface is important when modelling a sheet forming process.

For FEM to produce good results a good basis is needed. Amongst many other elements a mathematical base is needed to give a good result. For sheet metal forming a well described yield locus is needed to predict the form of the end product. Reality can be more accurately described by using a better definition for the yield locus. This thesis handles just this point.

At the *University of Twente* a test equipment is available to perform tests on sheet material. The tester is able to load a specimen on both shear and tensile force. With this equipment it is possible to measure the strains and stresses, and in this way, get a clear view on the yield surface.

1.2 Problem definition

The focus in this thesis is on the *biaxial tester*. Intuitively this testing system has great potential possibilities. The initial purpose was to explore the possibilities of the *biaxial tester*.

Soon however, it was discovered that one important variable in the measurements could not be measured, the transverse stress.

In this thesis the main target is to develop a method to determine the missing transverse stress. The method needs to be tested an validated.

1.3 Outline

In chapter 2 an introduction is given on the theory of plasticity, also the *biaxial tester* will be discussed in this section. It is concluded that one of the local stresses can not be determined. In the following chapter a new algorithm is presented that determines the missing transverse stress. This is done for both ideal and isotropic hardening plastic behaviour. In the fourth chapter the results from the various simulations are discussed. Here also the accuracy of the different simulations are investigated. Finally the conclusions and recommendations are presented.

Chapter 2

Theory and practise of plasticity

The goal of this thesis is to investigate what possible measurements can be done with the *biaxial tester*. Therefor an introduction on sheet material x is required as well as an introduction on the *biaxial tester*. The focus will be on material modelling as well as experimental tests with the *biaxial tester*.

In the first part of the chapter the theory of plasticity is discussed. By means of the tensile test the theory of plasticity is introduced and also two material models are considered. The second part of the chapter discusses the experimental side of plasticity by means of the *biaxial tester*. In this test a sample of sheet material is loaded in two directions. This way it is capable of producing a range of planar stress situations. The testing method is also discussed here. In the last section is investigated what the *biaxial tester* does measure. It is concluded that one of the local stresses is missing to define the plane stress situation.

2.1 Theory of plasticity

The theory of plasticity is best introduced on the basis of a uniaxial tensile test. This section is followed by a section that expands the uniaxial situation to a multi-axial stress state. After that two examples of yield criteria are considered.

2.1.1 The uniaxial situation

The uniaxial situation is best investigated with a normal tensile test. For such a test a specimen is used as depicted in Figure 2.1(a). The result of this test is shown in Figure 2.1(b).

For most metals the first part of the curve is linear. The deformation that occurs in this zone is called elastic; when the applied stress is removed the deformation is zero again. When deformation continues, the deformation will be plastic. The stress where elastic deformation x into plastic deformation is marked with the flow stress σ_{f}. When a material shows increasing resistance to further plastic deformation it hardens, this is illustrated by Figure 2.1(b). When the material does not harden during plastic deformation it is modelled as ideally plastic, this is depicted in Figure 2.1(c).

From Figure 2.1 the decomposition of the strain can be determined. The total strain is build up from an elastic part, and a plastic part. This is written as:

$$\varepsilon = \varepsilon^{\mathrm{p}} + \varepsilon^{\mathrm{e}} \qquad \Longleftrightarrow \qquad \dot{\varepsilon} = \dot{\varepsilon}^{\mathrm{p}} + \dot{\varepsilon}^{\mathrm{e}} \tag{2.1}$$

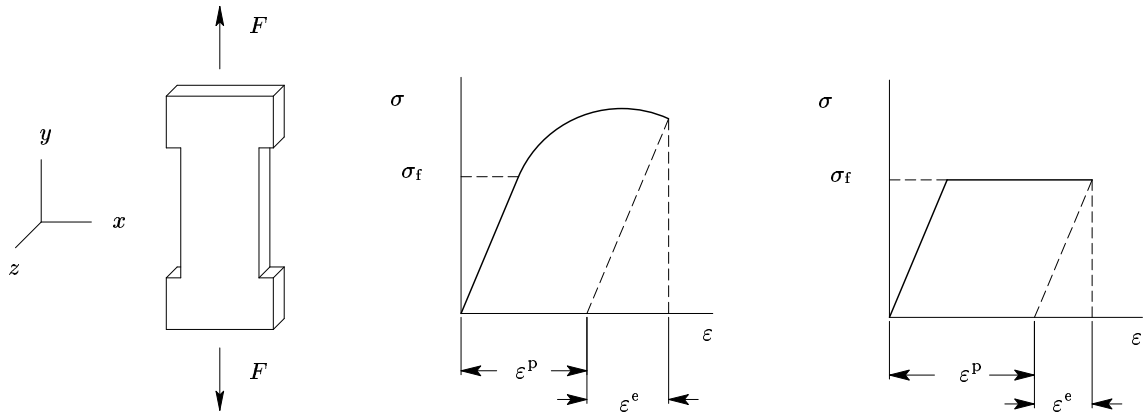

(a) The test sample (b) A hardening material (c) without hardening

Figure 2.1: The uniaxial tensile test

For metals, the elastic deformation is almost linear with respect to the stress. The Hookean law gives the relation between the stress σ and the elastic strain ε^{e}:

$$\sigma = E\varepsilon^{\mathrm{e}} \qquad \Longleftrightarrow \qquad \dot{\sigma} = E\dot{\varepsilon}^{\mathrm{e}} \tag{2.2}$$

The hardening is described as an increasing resistance to further plastic deformation. In the case that no hardening occurs, plastic deformation continues while the stress does not increase. A good approximation of a large part of the stress-strain curve can be obtained with a power law, *e.g.* the Ludwik-Nadai or Nadai relation:

$$\sigma_{\mathrm{f}} = C\left(\varepsilon^{\mathrm{p}} + \varepsilon_0\right)^n \tag{2.3}$$

With ε^{p} the plastic strain. If $n = 1$ linear hardening is modelled.

2.1.2 The multi axial situation

In practice, stress states are hardly ever uniaxial, so this asks for a multi axial description of the yield limit. In general, for three dimensional continuum mechanics it is common to derive the yield function in three dimensions, which results in six independent stresses. For sheet material however it is customary to neglect the three stresses normal to the plane σ_z, σ_{yz} and σ_{zx}. For all calculations in this thesis the three remaining stresses are used, σ_x, σ_y and σ_{xy}. So for plane stress situations the stress and strain vectors become

$$\boldsymbol{\sigma} = \left\{ \begin{array}{c} \sigma_x \\ \sigma_y \\ \sigma_{xy} \end{array} \right\} \qquad \boldsymbol{\varepsilon} = \left\{ \begin{array}{c} \varepsilon_x \\ \varepsilon_y \\ \gamma_{xy} \end{array} \right\} \tag{2.4}$$

The orientation of the axes are as in Figure 2.1(a).

The three planar stresses together form a three dimensional stress space. The yield surface is represented by some sort of sphere in this space. To get a better insight in the stresses, principal stresses are introduced (σ_1, σ_2). The local stress situation is rotated over an angle

θ, until the shear stress is zero. The two remaining stresses are normal stresses. This is illustrated in Figure 2.2 where a piece of sheet material is rotated so that only two normal stresses remain.

The principal stresses are calculated with the following equation

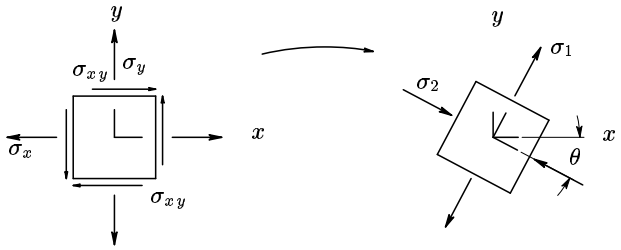

Figure 2.2: From local to principal stresses

$$\hat{\boldsymbol{\sigma}} = \mathbf{R} \cdot \boldsymbol{\sigma} \cdot \mathbf{R}^{\mathrm{T}} \tag{2.5}$$

With $\mathbf{R}$ a function of the angle θ. Commonly $\mathbf{R}$ is written in the matrix representation, $[R]$. The stresses in the elastic region are obtained from the generalised Hookean relation

$$\dot{\boldsymbol{\sigma}} = \mathbf{D} : \dot{\boldsymbol{\varepsilon}}^e \tag{2.6}$$

or, if the strains are required:

$$\dot{\boldsymbol{\varepsilon}}^e = \mathbf{C} : \dot{\boldsymbol{\sigma}} \tag{2.7}$$

in which the 4^{th}-order tensor represents the compliance tensor, with $\mathbf{C} = \mathbf{D}^{-1}$. In this case, the material behaviour is assumed to be isotropic and because sheet material is considered, the tensor $\mathbf{C}$ can be written in matrix representation

$$\mathbf{C} = \begin{bmatrix} \frac{1}{E} & -\frac{\nu}{E} & 0 \\ -\frac{\nu}{E} & \frac{1}{E} & 0 \\ 0 & 0 & \frac{1}{G} \end{bmatrix} \tag{2.8}$$

with the shear modulus $G = \frac{E}{2(1+\nu)}$.

As in the uniaxial situation the total strain is additively decomposed in a plastic and elastic component

$$\dot{\boldsymbol{\varepsilon}} = \dot{\boldsymbol{\varepsilon}}^e + \dot{\boldsymbol{\varepsilon}}^p \tag{2.9}$$

The description of plastic deformation in a multi axial stress state is somewhat harder to describe as the uniaxial situation. Therefor some extra entities are defined. Hardening is described by means of the equivalent stress and equivalent plastic strain. This is discussed in the following section. After that the flow stress (σ_{f}) is described in terms of the yield function. The last section is dedicated to the *principle of normality*.

Hardening

Since hardening laws are usually based on uniaxial measurements, these relations have to be expanded to a multi axial relation.

Customarily, hardening is described in two ways, isotropically and kinematically. If a material is characterised by isotropic hardening, the yield surface becomes proportionally larger. When a material is characterised by kinematic hardening the yield surface translates in the principal stress space. On the left-hand side of Figure 2.3 isotropic hardening is depicted, while on the right-hand side kinematic hardening is displayed. In Figure 2.3 the

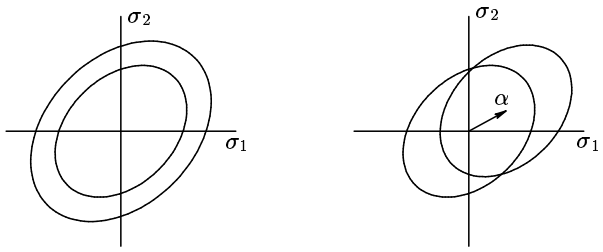

Figure 2.3: Isotropic (left) and kinematic (right) hardening

amount of kinematic hardening is described with the back stress tensor α which describes the displacement of the yield surface. Obvious, these are only models, in normal life hardening processes are much more complex.

From here on only isotropic hardening is discussed, because kinematic hardening is not used in this thesis. To describe this form of hardening two extra variables are introduced, the equivalent stress σ_{eq} and equivalent plastic strain $\varepsilon^{\text{p}}_{\text{eq}}$.

Because the shape of the yield surface does not change during plastic deformation, only the size does, a reference curve can be used to describe this process. Often a tensile test is used as the reference. The stresses and strains in such a test are then denoted as the equivalent stress and strain. Now the plastic strain vector $\boldsymbol{\varepsilon}^{\text{p}}$ and the stress vector $\boldsymbol{\sigma}$ must have some relation with their equivalents.

It is often assumed that the equivalent stress and strain pair should be energetically conjugate, see also [1]. The rate of plastic work is then described by

$$\dot{w}^p = \sigma_{\text{eq}}\dot{\varepsilon}^{\text{p}}_{\text{eq}} = \boldsymbol{\sigma} : \dot{\boldsymbol{\varepsilon}}^{\text{p}} \tag{2.10}$$

This then leads to the definition of the equivalent plastic strain rate:

$$\dot{\varepsilon}^{\text{p}}_{\text{eq}} = \frac{\boldsymbol{\sigma} : \dot{\boldsymbol{\varepsilon}}^{\text{p}}}{\sigma_{\text{eq}}} \tag{2.11}$$

The yield function

The three planar stresses from Equation (2.4) can be used to form a mathematical description of the yield surface. This leads to the yield function ϕ, where the yield surface is represented by $\phi = 0$. In the stress space, a stress state enclosed by the yield surface describes the elastic region. The stress state can not be outside the yield surface, by definition. The yield function can, however, change size and position, under the influence of plastic deformation, which is denoted by the equivalent plastic strain increment $\varepsilon^{\text{p}}_{\text{eq}}$.

This leads to a global definition of the yield function:

$$\phi\left(\boldsymbol{\sigma}\right) = \varphi\left(\boldsymbol{\sigma}\right) - \sigma_{\text{f}} \tag{2.12a}$$

$$\phi\left(\boldsymbol{\sigma}, \varepsilon_{\mathrm{eq}}^{\mathrm{p}}\right) = \varphi\left(\boldsymbol{\sigma}\right) - \sigma_{\mathrm{f}}\left(\varepsilon_{\mathrm{eq}}^{\mathrm{p}}\right) \tag{2.12b}$$

Where (2.12a) describes non hardening material and (2.12b) is used to describe isotropic hardening material. If $\phi < 0$ the material behaves elastically. When the yield function equals zero it represents the yield surface and the stress state is on it. Here plastic deformation occurs. Stress states where $\phi > 0$ can not occur.

Normality

In this section the relation between the yield surface and the plastic strain is observed. *Drucker's postulate* says that the complementary energy, derived from an arbitrarily stress cycle, is negative or equals zero. From *Drucker's postulate* it can be derived that the plastic strain is perpendicular to the yield surface, this is discussed in more detail in Appendix A.

In the space, spanned by σ, the gradient of the yield function is perpendicular to the yield surface ϕ. This leads to

$$\dot{\boldsymbol{\varepsilon}}^{\mathrm{p}} = \dot{\lambda}\frac{\partial \phi}{\partial \boldsymbol{\sigma}} \tag{2.13}$$

with $\dot{\lambda}$ a factor to scale both factors. The yield surface and the plastic strain are related to each other as depicted in Figure 2.4.

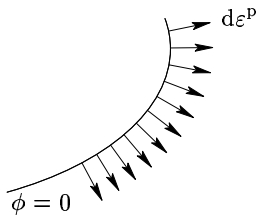

Figure 2.4: The plastic strain is perpendicular to the yield surface

2.1.3 Yield criteria

In this paragraph two well-known yield criteria are considered. The Von Mises criterion is used because it has roughly the same shape as the yield surface of steel. An advantage of this criterion is the easy to use mathematical description of the locus. The Vegter criterion is used because it is much more flexible. It describes a yield locus based on four tests, therefor it is better able to describe different shapes of yield loci.

The Von Mises criterion

This criterion is based on one test, *e.g.* the uniaxial test, which determines the size of the yield surface, the shape is determined in the criterion. Though the test is capable of describing the three dimensional situation, the criterion is derived for planar stress situations.

A simple notation of the criterion is:

$$\phi = \frac{3}{2}\mathbf{s} : \mathbf{s} - \sigma_{\mathrm{f}}^2 = 0 \tag{2.14}$$

in which the deviatoric stresses are denoted with **s**. This equation can be elaborated with total stresses instead of deviator stresses. Now the equation according to Huber and Hencky appears:

$$\phi = (\sigma_x - \sigma_y)^2 + (\sigma_y - \sigma_z)^2 + (\sigma_z - \sigma_x)^2 + 6\tau_{xy}^2 + 6\tau_{yz}^2 + 6\tau_{zx}^2 - 2\sigma_f^2 = 0 \tag{2.15}$$

In this last equation it can be clearly seen that the criterion is dependent on only one flow stress (σ_f). As was mentioned before in this thesis only the planar stresses are discussed. The stresses normal to the plane, σ_z, τ_{yz} and τ_{zx} are neglected. For Equation (2.15) this results in:

$$\tfrac{1}{2}\phi = \sigma_x^2 + \sigma_y^2 + 3\tau_{xy}^2 - \sigma_x\sigma_y - \sigma_f^2 = 0 \tag{2.16}$$

Equation (2.16) is the mathematical description of a spherical shape in the local stress space, see also Figure 2.5(a). These stresses can be converted to two principal stresses, which are

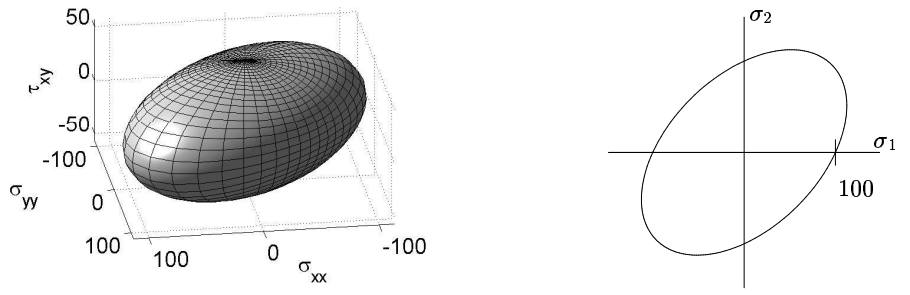

(a) The local stress space

(b) The principal stress space

Figure 2.5: The Von Mises representation in 2D and 3D with a yield stress of 100 N/mm^2

depicted in Figure 2.5(b). The Von Mises criterion is used in this thesis because it has an easy to handle mathematical description.

The Vegter criterion

A more sophisticated way of describing a yield surface is the method introduced by Vegter [3]. He developed a way to include four measurements in order to describe the yield locus more accurately. This model is specifically developed to describe planar stress situations. The model describes orthotropically behaviour and is symmetric around the origin. The performed tests are:

- simple shear test (SH)
- uniaxial test (UN)
- plane strain test (PS)
- equi-biaxial test (BI)

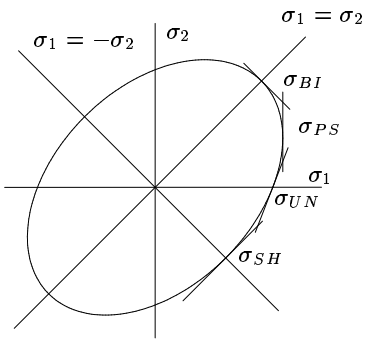

Figure 2.6: The Vegter yield surface with the four test points

The position of measurements in the stress space are indicated in Figure 2.6. In Appendix B these test are discussed in more detail. The intersection of the tangent lines define the hinge points. From these points the locus is interpolated. In this thesis only isotropic behaviour is considered, which means that the yield locus is symmetric about the lines $\sigma_1 = \sigma_2$ and $\sigma_1 = -\sigma_2$.

2.2 The biaxial tester

This section deals with the more experimental side of plasticity. For most experiments a uniaxial stress state is imposed. The *biaxial tester*, however, is a testing system that can load a specimen both on shear as on a tensile force. In this section the method is discussed.

2.2.1 The testing method

The tests are performed on a piece of sheet metal which is clamped at the upper and lower side of the sample. In Figure 2.7, the deformation zone is indicated as the narrow band in the centre of the sample. The lower clamp can translates in a vertical sense, the upper clamp translates in horizontal direction. Because the deformation zone has a high width-to-height ratio, the horizontal strain in the centre part of the deformation zone will remain zero, $\varepsilon_x = 0$. In this region a plane strain situation exists. On the right-hand side the local stress situation is depicted.

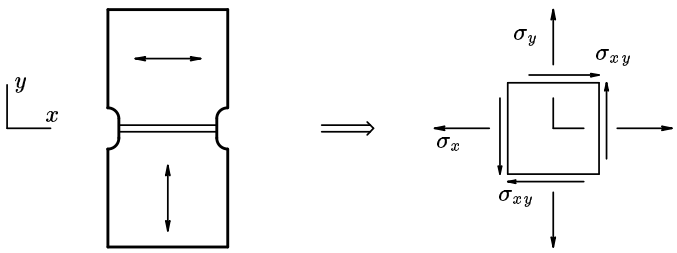

Figure 2.7: The sample and the stress situation

2.2.2 A survey of the test equipment

To get a clear view on the *biaxial tester*, the layout of the tester is depicted in Figure 2.8. The numbers in this picture correspond to the numbers in Table 2.1

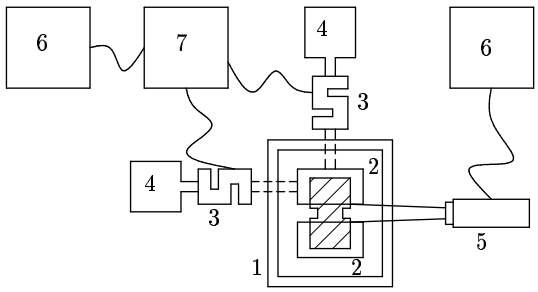

Figure 2.8: An overview on the biaxial system

#	description	#	description
1	central frame	5	camera
2	clamps	6	computers
3	force sensors	7	Galil controller
4	motors		

Table 2.1: Components of the *biaxial tester*

The test specimen (hatched) is loaded in two directions, shear and tensile. The lower clamp is constrained in the central frame, horizontally fixed. The upper clamp is able to translate in a horizontal sense, the lower clamp translates vertically. The forces are measured by the two force sensors.

The deformation is measured with a camera. On the test specimen four dots are applied, which are recorded with the camera. The information is sent to the computer where a macro runs that detects these dots and calculates their absolute position on the sheet. This information is used to determine the strains.

The advantage of measuring deformations with a camera instead of with displacement sensors on the clamps, is the exclusion of the stiffness of the central frame and the slip in the clamps. The sensors usually measure the displacement relative to the central frame, but since the central frame is also loaded, some elastic deformation occurs. This deformation is also measured by the sensors. The slip in the clamps though are responsible for the highest error in the measurements. The slip in the clamps will give an inaccuracy in the measured strains. By detecting the deformations directly from the specimen the elastic deformation of the frame and the slip in the clamps is bypassed.

2.2.3 Specifications of the biaxial tester

In the former section an overview was given on how the *biaxial tester* works, in this section a more detailed look is given to the tester.

Sample

The *biaxial tester* is meant for experiments with aluminium and steel. For steel however, the region to be deformed can not be too thick, otherwise the required force would be too high. This would then lead to damage to the *biaxial tester*. In Figure 2.9 a regular sample is

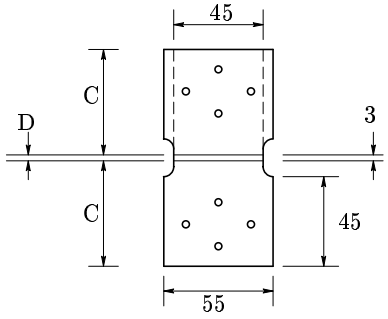

Figure 2.9: Sample

depicted. The sample is clamped at both ends, where the height C indicates the clamped part of the sample. This leaves a horizontal area D open to perform the actual measurements. In Pijlman [2] it is demonstrated that the centre part of this area, in horizontal sense, displays a plain strain situation when it is loaded. At the left- and right-hand side of the sample this plane strain state is not achieved. Measurements are performed on the center part of the deformation zone.

The accuracy

In order to gain reliable result from the *biaxial tester* the machine is tested on it's accuracy. In the dissertation of Pijlman [2] the complete description is given on all specific parts. In this thesis only the final results are given, see Table 2.2. A large influence on the accuracy

	Plane strain	Shear test
stress	2.6%	1%
strain	1.6%	0.8%
minimal strain	0.016 [-]	0.011 [-]

Table 2.2: Stress and strain accuracy.

for both the stress and the strain is the dot size in relation to the number of pixels on the camera. If the dots get smaller, the accuracy of the two mentioned quantities grow. This is also the case with the camera, when the number of pixels is increased, accuracy is gained.

2.3 The stress state during tests

In this section an inventory is made of all the variables that are measurable. Intuitively, the *biaxial tester* can cover a large part of the stress space. In this section it is investigated what area is accessible and if all the quantities can be determined from the test. It will be shown that the transverse stress σ_x can not be measured or determined directly.

2.3.1 The covered stress domain

In this section the covered stress domain of the *biaxial tester* is investigated. In the local stress space this can be represented with a 3D surface, in the principal stress it is represented by the yield locus. To get a clear picture on the situation, both are discussed in this section. At first the *shear point* is discussed, after which the *plane-strain point* is investigated. After that an arbitrarily stress state applied by the *biaxial tester* is discussed.

Applying a simple shear load to a specimen results in a situation as depicted in Figure 2.11(a). The angle θ between the principal axes and the local axes is 45°, which is reflected in Figure 2.11(b). Because the material is assumed to behave elastic planar istropically, the principal stresses are equal in magnitude, but are oppositely orientated. This is also illustrated by Figure 2.11(c). In the local stress space, the stress state is on top of the sphere, see Figure 2.10.

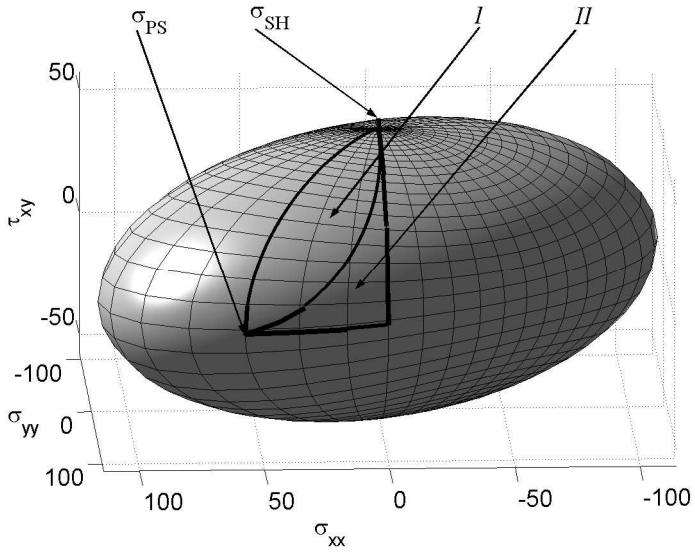

Figure 2.10: The 3D local stress space

Because of the high width-to-height ratio, a tensile force leads the stress state to the *plane-strain point*, Figure 2.12 illustrates this test. It is noticed that in this situation, the local stresses have the same orientation as the principal stresses. Figure 2.10 illustrates this, the *plane-strain point* is on the level where the shear stress equals zero, which is just the definition of principal stresses.

The former two situations have led the stress state to a well definied state, the *shear point* or the *plane-strain point*. No matter the magnitude of the deformation, the stress state will always be at the *plane-strain point* or the *shear point*. For a loading situation where both a shear and a tensile force are arbitrarily applied, the stress state is not fixed to a certain position. The position of the stress state depends on the amount of shear and tensile deformation, and the ratio between them. The angle between the local axes and the principal axes varies from 45° to 0°.

In the principal stress space the boundaries that limit the stress domain covered by the *biaxial tester*are clear; the yield locus between the *shear point* and the *plane-strain point*. In

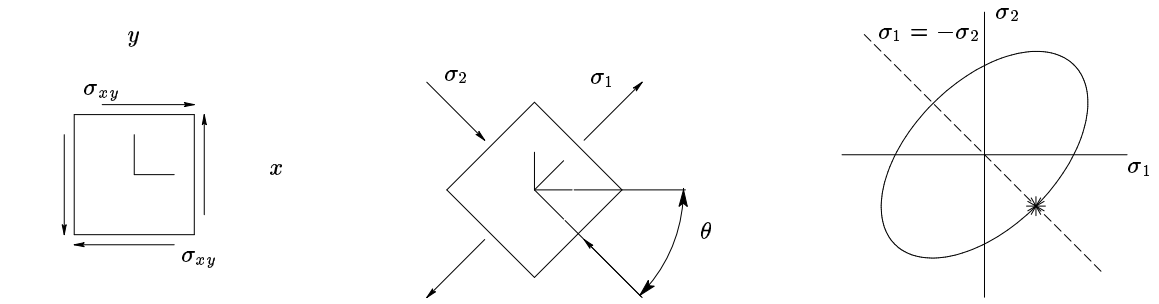

(a) The local stresses (b) The principal stresses (c) The principal stress space

Figure 2.11: A shear force applied to the sample

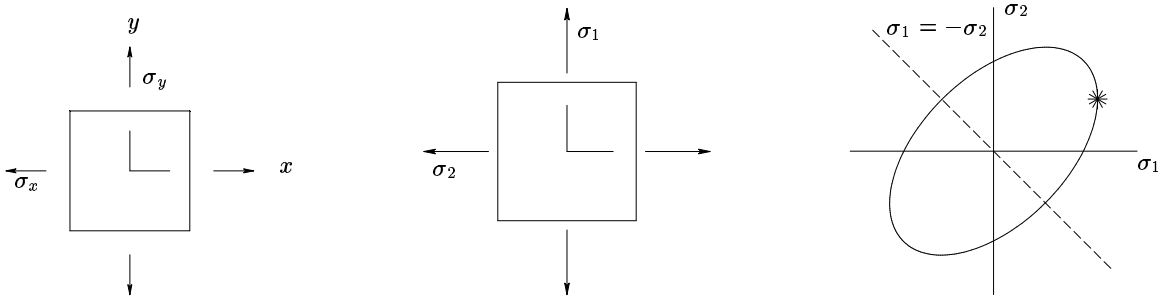

(a) The local stresses (b) The principal stresses (c) The principal stress space

Figure 2.12: A set of tensile forces applied to the sample

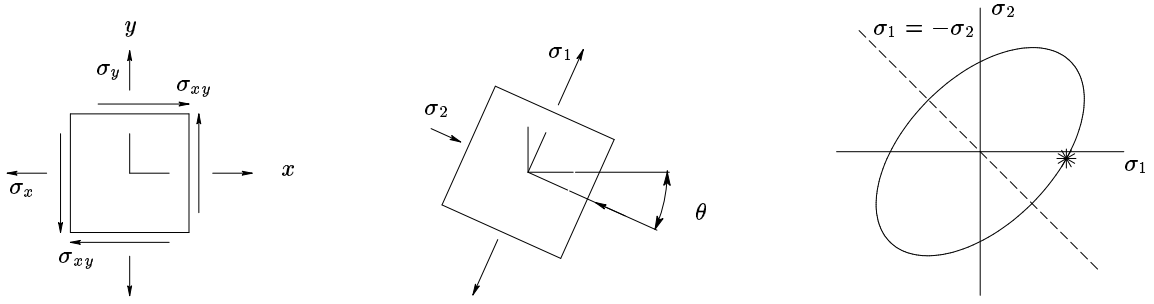

(a) The local stresses (b) The principal stresses (c) The principal stress space

Figure 2.13: A shear and tensile force applied to the sample

the local stress space this is not so obvious. In Figure 2.10 two area's are depicted, *I* and *II*. The outer limits of the total area is formed by three planes. These are the planes defined by $\sigma_x = 0$, $\sigma_{xy} = 0$ and the vertical plane for which the normal on the yieldsurface has *no*

positive component in the σ_x-direction. A negative component in the σ_x-direction would lead to a positive plastic deformation in the lateral direction, which is not possible. Area I is the area that the *biaxial tester* really covers. The size of the domain is determined by the *Poisson's ratio*, μ. A relative high ratio, results in stress states nearby the left-hand side of the area. A relatively low ratio will result in a curve that separates area I and II. When a specimen is sheared in the negative direction the lower half of the sphere is covered just as the upper half is.

2.3.2 Inventory of measurable quantities

The possible measurements discussed in the former section give a good opportunity to gain information on the yield surface and on hardening parameters.

Now that is reasoned which area of the stress and strain space the *biaxial tester* can cover, it has to be investigated if all the necessary quantities can be measured from the test equipment. As was briefly mentioned this is not the case. In Table 2.3 the variables are listed. These quantities can be converted to more usable quantities such as strains and stresses.

variable	unit	description
u_c	mm	horizontal movement of the upper clamp
v_c	mm	vertical movement of the lower clamp
u_i	mm	horizontal coordinate of dot i
v_i	mm	vertical coordinate of dot i
F_x	N	Force in horizontal(x) direction
F_y	N	Force in vertical(y) direction
t	s	Time

Table 2.3: Measured variables during testing.

In Table 2.4 these quantities are listed. Remarked is that for all the quantities also their

quantity	derived from
σ_y [N/mm^2]	F_y and b
σ_{xy} [N/mm^2]	F_x and h
ε_y [-]	u_1 ... u_4
ε_x [-]	u_1 ... u_4
γ_{xy} [-]	u_1 ... u_4

Table 2.4: Converted quantities from the measured quantities

timederivates can be determined. For the clearness of the table this is left out.

One important problem that occurs under these circumstances is that the available variables do not give enough information to calculate the principal stresses. The principal stresses (σ_1, σ_2) are determined from Equation 2.5. Elaborating this equation for the planar stress situation gives:

$$\begin{bmatrix} \sigma_1 & 0 \\ 0 & \sigma_2 \end{bmatrix} = [R(\theta)] \begin{bmatrix} \sigma_x & \sigma_{xy} \\ \sigma_{yx} & \sigma_y \end{bmatrix} [R(\theta)]^T \tag{2.17}$$

Because $\sigma_{xy} = \sigma_{yx}$ this set of equations leads to two independent equations. The missing variables which have to be calculated are σ_1, σ_2, and σ_x. An extra equation is needed to compute all variables.

2.3.3 Conclusion

In this section an inventory is made of all quantities that can be measured. Also the regions where the *biaxial tester* intuitively should be able to perform measurements are discussed.

The most important conclusion is that one stress component is missing. The outcome of this is that the principal stresses can not be calculated. This throws the *biaxial tester* back to a simple shear tester and a tensile tester. In other words, the advantage of the *biaxial tester*, being able to perform loads in two directions, is lost in the process.

During my graduation process a theoretical procedure was developed that determines this missing transverse stress. In the next chapter this algorithm is treated.

Chapter 3

The transverse stress algorithm

The former chapter ended with the conclusion that the transverse stress can not be directly determined from the measurements. In this chapter an algorithm is introduced that calculates the transverse stress. The method uses the total differential of the yield function and the *principle of normality* as a starting point.

In the first section the principles of the method are discussed. In the second section the mathematical description of the algorithm is presented for non-hardening behaviour. After that the algorithm with hardening is discussed. In the last section the simulations are discussed.

3.1 Introducing the principles of the algorithm

In this section the principles of the algorithm are introduced.

The algorithm is based on the *principle of normality*, which says that the direction of the plastic strain is perpendicular to the yield surface ϕ. This is shown in Figure 3.1(a).

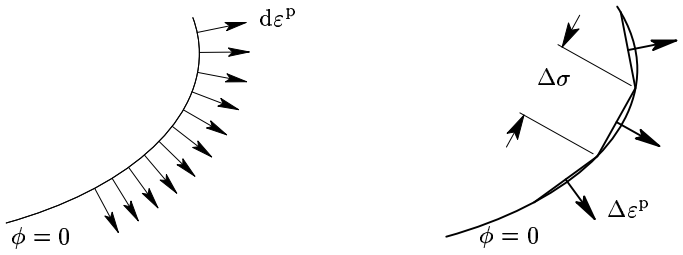

(a) Continous (b) Incremental

Figure 3.1: The plastic strain is perpendicular to the yield surface

The algorithm is applied on a test on the *biaxial tester*. This test consists of two parts. The first part is a shearing step which leads the stress state "onto" the yield locus. In the second part the specimen is vertically strained. During this deformation the stress state moves upwards in the principal stress space along the yield surface. Once the stress state is on the yield surface it stays on the yield surface during deformation.

The test is performed on a specimen that behaves elastic planar isotropically. The initial stresses and strains are zero. The first deformation step is shearing the specimen. The shear stress σ_{xy} is measured directly. The transverse stress σ_y is also measured directly but should equal zero because only a shear stress is imposed. With this in mind, three situations for the transverse stress are possible, these are denoted by Mohr's circles in Figure 3.2. In the

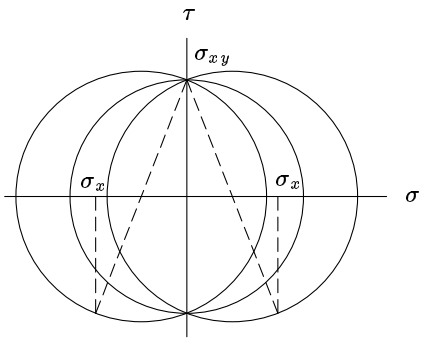

Figure 3.2: Mohr's circles for simple shear

left-hand circle the transverse stress is smaller than zero, in the right-hand circle it is greater than zero. The circle in the middle represents the situation where σ_x equals zero. Because the material is assumed to be elastic planar isotropic, the left- and right-hand situation are not possible. They would imply a strain in transverse direction, which is in contradiction with the definition of elastic planar isotropically when the vertical strain equals zero. This step should lead the stress state "just on" the yield surface. In this step all the quantities are known, or can be determined.

Now the second part of the deformation process starts. The following deformation step is in vertical direction imposed on the specimen. The stress state can no longer be calculated with Mohr's circles, because the transverse stress is missing. Also the angle θ between the local and principal system is unknown, which is illustrated in Figure 3.3.

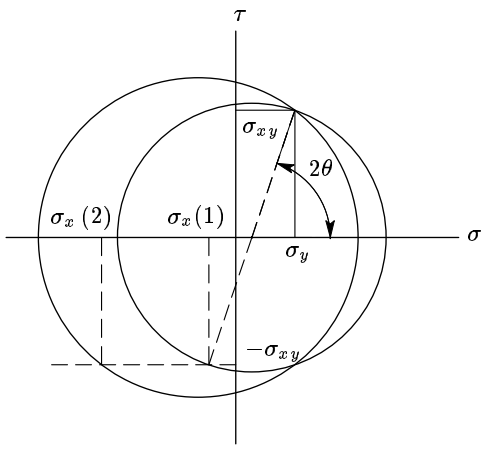

Figure 3.3: Different circles for different values of the unknown transverse stresses $\sigma_x(i)$ and the unknown angle θ

Here the *principle of normality* comes in. The *principle of normality* states that the plastic strain is perpendicular to the yield surface. If a small step is made along the yield surface, by applying the vertical displacement, the plastic strain that results from this deformation should be perpendicular to the stress increment. Because the deformation stays plastic, the *principle of normality* can be used to determine the transverse stress. Now only the plastic strains have to be determined.

But here another problem arises. While plastic deformation continues, hardening occurs in most metals. As a consequence, the yield locus translates or increases. When a material hardens, the yield locus after a deformation step is different from the yield locus before this deformation step. This is illustrated in Figure 3.4.

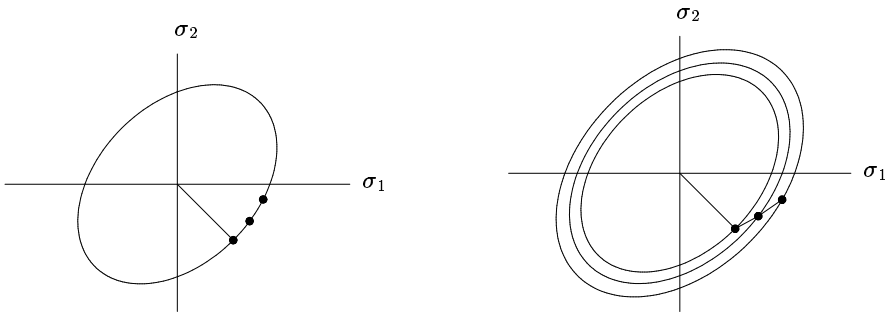

(a) Stress path without hardening

(b) Stress path with hardening

Figure 3.4: Stress paths for a non hardening and a isotropically hardening material.

If hardening is not included in the model, the plastic strains can be determined from the stresses by means of the compliance matrix and the decomposition of the strain in an elastic and plastic part. If hardening is included this is somewhat more difficult.

For this thesis only isotropic hardening is considered. The growth of the yield locus is determined with a tensile test. This test, which is done separately from the test in the *biaxial tester*, serves as a reference for the hardening. The increase in stress as a result of the hardening is translated to an increase in size of the yield locus. This is illustrated in Figure 3.5.

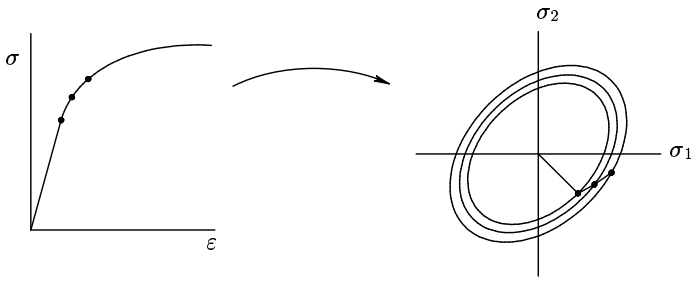

Figure 3.5: Hardening as demonstrated in a tensile test is used to describe isotropic hardening.

3.2 Algorithm without hardening

In the former section a description was given on the algorithm, in this section the mathematical description of the algorithm is discussed.

As said before, since sheet material is studied, only planar stresses are discussed, the other stresses are neglected. The equivalent strain is no variable of the yield function, because hardening is not included. The yield function from Equation (2.12a) is used

$$\phi = \phi(\boldsymbol{\sigma}) = \varphi(\boldsymbol{\sigma}) - \sigma_{\mathrm{f}} \tag{3.1}$$

In this equation φ is a homogeneous function of the first order. During the test it is assumed that the stress state is on the yield surface, so plastic deformation occurs and

$$\phi = \phi(\boldsymbol{\sigma}) = 0 \tag{3.2}$$

From which it follows that

$$\mathrm{d}\phi = \frac{\partial \phi}{\partial \varphi}\frac{\partial \varphi}{\partial \boldsymbol{\sigma}} : \mathrm{d}\boldsymbol{\sigma} = 0 \tag{3.3}$$

Because the yield function is defined as in (3.1), the first fraction in (3.3) equals 1. Now Equation (3.3) is multiplied with $\dot{\lambda}$

$$\dot{\lambda}\frac{\partial \phi}{\partial \boldsymbol{\sigma}} : \mathrm{d}\boldsymbol{\sigma} = 0 \tag{3.4}$$

After substitution of (2.13) in (3.4) the last equation becomes

$$\dot{\boldsymbol{\varepsilon}}^{\mathrm{p}} : \mathrm{d}\boldsymbol{\sigma} = 0 \tag{3.5}$$

Now (3.5) is discretised. The plastic strain rate $\dot{\boldsymbol{\varepsilon}}^{\mathrm{p}}$ is written as $\frac{\mathrm{d}\boldsymbol{\varepsilon}^{\mathrm{p}}}{\mathrm{d}t}$. The mean plastic strain rate $\dot{\boldsymbol{\varepsilon}}^{\mathrm{p}}_{\mathrm{m}}$ can be elaborated in terms of the strain between two points i and j

$$\dot{\boldsymbol{\varepsilon}}^{\mathrm{p}}_{\mathrm{m}} = \frac{\boldsymbol{\varepsilon}^{\mathrm{p}}(j+1) - \boldsymbol{\varepsilon}^{\mathrm{p}}(j)}{t(j+1) - t(j)} = \frac{\boldsymbol{\varepsilon}^{\mathrm{p}}(j+1) - \boldsymbol{\varepsilon}^{\mathrm{p}}(j)}{\Delta t} \tag{3.6}$$

When the mean plastic strain rate is taken over an infinite small increment, the time increment approaches zero and the strain increment decreases

$$\lim_{\Delta t \to 0} \dot{\boldsymbol{\varepsilon}}^{\mathrm{p}}_{\mathrm{m}} = \lim_{\Delta t \to 0} \frac{\boldsymbol{\varepsilon}^{\mathrm{p}}(j+1) - \boldsymbol{\varepsilon}^{\mathrm{p}}(j)}{\Delta t} = \dot{\boldsymbol{\varepsilon}}^{\mathrm{p}} \tag{3.7}$$

So, if the increments are taken small enough, the mean plastic strain rate approaches the plastic strain rate. The stress increment $\mathrm{d}\boldsymbol{\sigma}$ is substituted by $\Delta\boldsymbol{\sigma}$. Every change in the stress state is directly related to a plastic strain increment.

$$\Delta\boldsymbol{\varepsilon}^{\mathrm{p}} : \Delta\boldsymbol{\sigma} = 0 \tag{3.8}$$

With (2.9) the plastic strain increment can be written in terms of total and elastic strain

$$(\Delta\boldsymbol{\varepsilon} - \Delta\boldsymbol{\varepsilon}^{\mathrm{e}}) : \Delta\boldsymbol{\sigma} = 0 \tag{3.9}$$

And with the elastic constitutive behaviour from (2.7), this becomes

$$(\Delta\boldsymbol{\varepsilon} - \mathbf{C}\Delta\boldsymbol{\sigma}) : \Delta\boldsymbol{\sigma} = 0 \tag{3.10}$$

This can be elaborated in terms of $\Delta\sigma_x$. For the plane stress situation $\Delta\sigma_y$, $\Delta\sigma_{xy}$, $\Delta\varepsilon_x$, $\Delta\varepsilon_y$ and $\Delta\gamma_{xy}$ are known from the tests. So, for elastically isotropic behaviour Equation (3.10) yields

$$\begin{aligned} &-\tfrac{1}{E}\left(\Delta\sigma_x\right)^2 + \left(\Delta\varepsilon_x + \tfrac{2\nu\Delta\sigma_y}{E}\right)\Delta\sigma_x \\ &+ \left(\Delta\varepsilon_y - \tfrac{\Delta\sigma_y}{E}\right)\Delta\sigma_y + \left(\Delta\gamma_{xy} - \tfrac{\Delta\sigma_{xy}}{G}\right)\Delta\sigma_{xy} = 0 \end{aligned} \tag{3.11}$$

This quadratic equation in $\Delta\sigma_x$ is used to calculate the stress σ_x at the end of each increment. The initial conditions of the increment must be known. This is the case when the first step is simple shear. At that point σ_x equals zero. From here on the following points can be calculated, as long as the stress state is "on" the yield surface. Otherwise Equation (3.3) is no longer valid, because then $\mathrm{d}\phi \neq 0$.

3.3 Algorithm with hardening

In this section the algorithm described in Section 3.2 is expanded with hardening. This contributes to the practical value of the algorithm. Only isotropic hardening is discussed.

As discussed in Chapter 2 the yield locus can be described as a function of the stresses and the equivalent plastic strain.

$$\phi = \phi\left(\boldsymbol{\sigma}, \varepsilon^{\mathrm{p}}_{\mathrm{eq}}\right) \tag{3.12}$$

And if plastic deformation occurs, from (2.12b)

$$\phi = \phi\left(\boldsymbol{\sigma}, \varepsilon^{\mathrm{p}}_{\mathrm{eq}}\right) = \varphi\left(\boldsymbol{\sigma}\right) + \sigma_{\mathrm{f}}\left(\varepsilon^{\mathrm{p}}_{\mathrm{eq}}\right) = 0 \tag{3.13}$$

And

$$\mathrm{d}\phi = \frac{\partial\phi}{\partial\varphi}\frac{\partial\varphi}{\partial\boldsymbol{\sigma}}\mathrm{d}\boldsymbol{\sigma} - \frac{\partial\phi}{\partial\sigma_{\mathrm{f}}}\frac{\partial\sigma_{\mathrm{f}}}{\partial\varepsilon^{\mathrm{p}}_{\mathrm{eq}}}\mathrm{d}\varepsilon^{\mathrm{p}}_{\mathrm{eq}} = 0 \tag{3.14}$$

The left-hand term of the equation is discussed in the former section. The right-hand term is discussed in this section. Again the purpose is to write all variables as a function of the missing transverse stress.

The first fraction $(\partial\phi/\partial\varphi)$ equals -1, because it is defined as in (3.13). The second fraction is the derivative of the tensile test, at the calculated flow stress. This is based on the data acquired from the tensile test. From Equation (2.11) the rate of equivalent plastic strain can be determined

$$\dot{\varepsilon}^{\mathrm{p}}_{\mathrm{eq}} = \frac{\boldsymbol{\sigma} : \dot{\boldsymbol{\varepsilon}}^{\mathrm{p}}}{\sigma_{\mathrm{eq}}} \tag{3.15}$$

If plastic deformation occurs, the equivalent stress is equal to the current flow stress. Now discretisation takes place, with $\dot{\varepsilon}^{\mathrm{p}}_{\mathrm{eq}}$ being replaced by $\Delta\varepsilon^{\mathrm{p}}_{\mathrm{eq}}$ as in the former section. The plastic strain rate $\dot{\boldsymbol{\varepsilon}}^{\mathrm{p}}$ is substituted by $\Delta\boldsymbol{\varepsilon}^{\mathrm{p}}$. This leads to

$$\Delta\varepsilon^{\mathrm{p}}_{\mathrm{eq}} = \boldsymbol{\sigma} : \frac{\Delta\boldsymbol{\varepsilon}^{\mathrm{p}}}{\sigma_{\mathrm{eq}}} \tag{3.16}$$

This is then substituted into the second term of Equation (3.14):

$$\frac{\partial\phi}{\partial\sigma_{\mathrm{f}}}\frac{\partial\sigma_{\mathrm{f}}}{\partial\varepsilon^{\mathrm{p}}_{\mathrm{eq}}}\mathrm{d}\varepsilon^{\mathrm{p}}_{\mathrm{eq}} = -h\frac{\boldsymbol{\sigma}}{\sigma_{\mathrm{eq}}} : \Delta\boldsymbol{\varepsilon}^{\mathrm{p}} \tag{3.17}$$

In which h stands for $\frac{\partial \sigma_f}{\partial \varepsilon_{eq}^p}$, which is the hardening rate.

When the result from the former section is included, Equation (3.10), then Equation (3.14) will have the following form

$$(\Delta\boldsymbol{\varepsilon} - \mathbf{C}\Delta\boldsymbol{\sigma}) : \Delta\boldsymbol{\sigma} - h\frac{\boldsymbol{\sigma}}{\sigma_{eq}} : \Delta\boldsymbol{\varepsilon}^p = 0 \tag{3.18}$$

From which it follows that

$$(\Delta\boldsymbol{\varepsilon} - \mathbf{C}\Delta\boldsymbol{\sigma}) : \left(\Delta\boldsymbol{\sigma} - h\frac{\boldsymbol{\sigma}}{\sigma_{eq}}\right) = 0 \tag{3.19}$$

As in the algorithm without hardening this is a quadratic function in $\Delta\sigma_x$, when $\boldsymbol{\sigma}$, σ_{eq} and h are constant during a step. The flow stress is updated after each step by means of the equivalent plastic strain increment. The flow stress then becomes

$$\sigma_f = \sigma_f\left(\varepsilon_{eq}^p\right) \tag{3.20}$$

This relation is determined from a separately performed uniaxial tensile test.

The first step in the deformation process is used to get the stress state on the yield locus. This step should not initiate plastic deformation. The stress state has to be "just" on the yield locus, otherwise the equivalent plastic strain rate increases and also the flow stress. After this the next deformation part is started. For every strain increment in vertical direction the equivalent plastic strain rate has to be calculated. By means of the equivalent plastic strain rate the equivalent stress is updated. So after each step the flow stress is calculated. Following this procedure the path, covered in the principal stress space, can be determined.

This algorithm is only valid when plastic deformation occurs, otherwise Equation (3.19) does not hold anymore.

3.4 The choice of the correct solution

In the former two sections the algorithm is discussed. Both algorithms use quadratic equations in $\Delta\sigma_x$. As a consequence, two solutions are possible. On the basis of (3.11) the correct solution is determined in this section.

At first instance an interval method was used to determine the stress σ_x. But after a closer look to the whole algorithm, the expression where the missing stress is calculated, appears to be a simple second order equation in terms of $\Delta\sigma_x$. From the algorithm without hardening the quadratic equation is used, (3.11)

$$\begin{aligned} \Delta\phi &= a\,\sigma_x^2 + b\,\sigma_x + c \qquad \text{with} \\ a &= -\tfrac{1}{E} \\ b &= \Delta\varepsilon_x + 2\tfrac{\nu}{E}\Delta\sigma_y \\ c &= \left(\Delta\varepsilon_y - \tfrac{\Delta\sigma_y}{E}\right)\Delta\sigma_y + \left(\Delta\gamma_{xy} - \tfrac{\Delta\sigma_{xy}}{G}\right)\Delta\sigma_{xy} \end{aligned} \tag{3.21}$$

In which the total transverse strain equals zero, because a plane strain situation is assumed, and thus is left out of the following equations. The two roots of this quadratic equation in $\Delta\sigma_x$ are:

$$\begin{aligned} (\Delta\sigma_x)_1 &= \nu\Delta\sigma_y - \sqrt{(\nu^2-1)\,\Delta\sigma_y^2 + E\Delta\varepsilon_y\Delta\sigma_y - 2\,(\nu+1)\,\Delta\sigma_{xy}^2 + E\Delta\gamma_{xy}\Delta\sigma_{xy}} \\ (\Delta\sigma_x)_2 &= \nu\Delta\sigma_y + \sqrt{(\nu^2-1)\,\Delta\sigma_y^2 + E\Delta\varepsilon_y\Delta\sigma_y - 2\,(\nu+1)\,\Delta\sigma_{xy}^2 + E\Delta\gamma_{xy}\Delta\sigma_{xy}} \end{aligned} \tag{3.22}$$

The next question is which one to choose? The answer is found in the calculation of the strains. The elastic strain for the transverse (x) direction is determined from Hooke's law

$$\Delta\varepsilon_x^{\mathrm{e}} = \frac{1}{E}\Delta\sigma_x - \frac{\nu}{E}\Delta\sigma_y \tag{3.23}$$

The results for the two possible solutions are:

$$\begin{aligned}(\Delta\varepsilon_x^{\mathrm{e}})_1 &= -\sqrt{(\nu^2-1)\,\Delta\sigma_y^2 + E\Delta\varepsilon_y\Delta\sigma_y - 2\,(\nu+1)\,\Delta\sigma_{xy}^2 + E\Delta\gamma_{xy}\Delta\sigma_{xy}} \\ (\Delta\varepsilon_x^{\mathrm{e}})_2 &= \sqrt{(\nu^2-1)\,\Delta\sigma_y^2 + E\Delta\varepsilon_y\Delta\sigma_y - 2\,(\nu+1)\,\Delta\sigma_{xy}^2 + E\Delta\gamma_{xy}\Delta\sigma_{xy}}\end{aligned} \tag{3.24}$$

The term under the radical sign is positive and as a result the root is real.

The elastic strain increment can have a positive or negative value. The total strain in transverse direction is zero and therefore the plastic strain increment has the same value as the elastic strain increment, but with opposite sign. For the first solution this would mean that the plastic strain increment in transverse direction is positive. Hence, the plastic strain in transverse direction is increasing during testing. However, in the measured area in the principal stress space, the plastic strain in transverse direction, should be negative. This is illustrated in Figure 3.6[1]. From the first step on the yield locus, the plastic strain

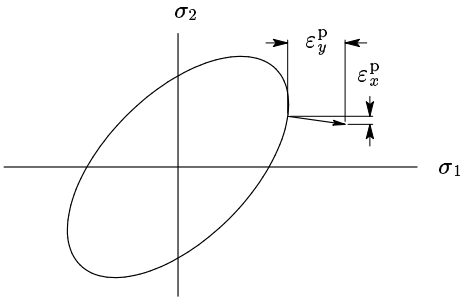

Figure 3.6: The transverse strain is negative

should be negative, otherwise the plastic strain would directly have a positive value. Another consequence is that the transverse stress would be smaller than zero. In a more intuitive reasoning this is also impossible. Without the plane strain constraint, the material would expose a negative lateral contraction; the size of the loaded region increases in both vertical and horizontal sense.

As a result the elastic strain has to be negative, and so the second solution gives the correct answer. For the algorithm with hardening the same procedure is followed and here also the second (and positive) solution is the correct one.

3.5 Test sequence

The presented algorithm is developed for the *biaxial tester*. But since the equipment was upgraded during the graduation project, there was no possibility to perform real tests. Therefore,

[1] because the principal and local stress space have almost the same orientation, the local strains are depicted in the figure, *not* the plastic strains as a result from the principal stresses

simulations are performed. The practical side of the tests are done in DIEKA, to simulate the *biaxial tester*. The results from these simulations are σ_x, σ_y, σ_{xy}, ε_x, ε_y and γ_{xy}. The algorithm is implemented in MATLAB, where the results from the DIEKA simulations, but *not* σ_x, are used to calculate σ_x. After that the calculated stress σ_x from MATLAB and the 'exact' stress, calculated by DIEKA, are compared.

3.5.1 Dieka simulation

In this paragraph the input in DIEKA is discussed. Started is with the modelling of the sample.

The sample as it is used in the *biaxial tester* is quite large. For the DIEKA simulation the sample is not entirely modelled. As explained before the deformation zone is only loaded on a tensile and shear force. In order to keep things as easy as possible, only a square element is modelled. The advantage of this method is that the strains are easily calculated. The area spanned by the four dots on the sample is the same as the area spanned by the elements in DIEKA (1 x 1 mm).

When loading the sample with a tensile load, the horizontal strain will equal zero. Because the sample has a large width-to-height ratio, the centre of the sample will not be able to deform in the horizontal direction. In other words, the material above and below the centre prevents it from deforming. The place where horizontal deformation will occur is at the sides of the sample. The model will be constrained as to simulate this property. The layout of the simulation can be seen in Figure 3.7.

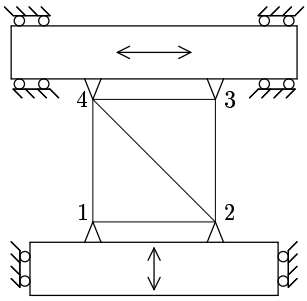

Figure 3.7: The modelled elements in DIEKA

The way that DIEKA calculates strains also influences the result, therefore a short discussion on this subject follows. In Figure 3.8 the principal stress space is depicted with an arbitrarily yield locus and a stress state (i) within the elastic region. When a deformation is prescribed, a temporary stress state is calculated as if the deformation is fully elastic. The stress state translates in the principal stress space to the temporary stress $\boldsymbol{\sigma}^{\mathrm{t}}$

$$\boldsymbol{\sigma}^{\mathrm{t}} = \boldsymbol{\sigma}_i + \mathbf{D}\Delta\boldsymbol{\varepsilon} \tag{3.25}$$

Since this temporary stress state is outside the yield locus, plastic strain occurs. Also, the elastic law $\mathbf{D}$ is not valid in the plastic region. The succeeding stress state is written in terms of elastic strains

$$\boldsymbol{\sigma}_{i+1} = \boldsymbol{\sigma}_i + \mathbf{D}\Delta\boldsymbol{\varepsilon}^{\mathrm{e}} \tag{3.26}$$

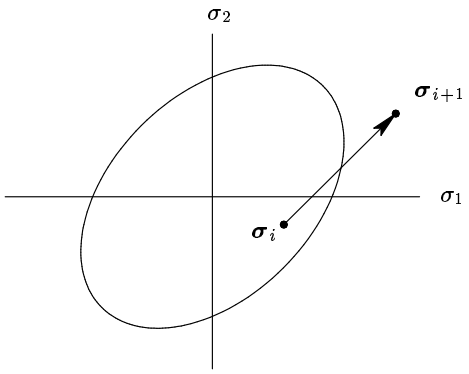

Figure 3.8: The stress state translates under influence of deformation

and with the decomposition of the total strain:

$$\boldsymbol{\sigma}_{i+1} = \boldsymbol{\sigma}_i + \mathbf{D}\left(\Delta\boldsymbol{\varepsilon} - \Delta\boldsymbol{\varepsilon}^{\mathrm{p}}\right) \tag{3.27}$$

In this equation the temporary stress is recognised:

$$\boldsymbol{\sigma}_{i+1} = \boldsymbol{\sigma}^{\mathrm{t}} - \mathbf{D}\Delta\boldsymbol{\varepsilon}^{\mathrm{p}} \tag{3.28}$$

At this point the relation between the yield surface and the plastic strain increment is used, (2.13)

$$\boldsymbol{\sigma}_{i+1} = \boldsymbol{\sigma}^{\mathrm{t}} - \lambda\mathbf{D}\left(\frac{\partial\phi}{\partial\boldsymbol{\sigma}}\right) \tag{3.29}$$

This equation is iteratively solved, in this way, the plastic strain is perpendicular to the yield surface. The difficulty with this equation is which $\boldsymbol{\sigma}$ to choose in the differential equation? For stability reasons the stress at $(i+1)$ is chosen. As a result the plastic strain is calculated at the end of the increment, and not the mean value of the increment. This is illustrated in Figure 3.9. For the proposed algorithm, where the stress state moves along the yield

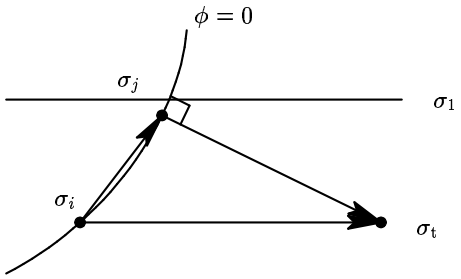

Figure 3.9: The plastic strain increment is determined at the end of the increment

locus, this needs to be compensated for. When large increments are used in DIEKA, an error is made in the calculation of the differential equation. This can be corrected by using small increments in DIEKA. For the validation of the algorithm, small increments are used in DIEKA, the algorithm then uses *e.g.* 10 DIEKA increments for it's calculation.

This problem will not occur when the tests on the *biaxial tester* are performed. Here the plastic strain is always perpendicular to the yield surface. So, in practice, not so much effort has to be made to reach the same level of accuracy.

3.5.2 Implementation in MatLab

The algorithm as it is implemented in MATLAB does not differ much from the proposed algorithm. The main difference is the computation of the total strain.

The strains

At two places the strains need to be calculated. The first is when the deformations have to be converted to total strains. The other place is where the plastic strain is computed.

Relatively much attention is paid to this subject because it has quite some influence on the final result. This is due to the incremental way of calculating. If a structural error is made in the algorithm, the error made in the first step will have an influence on the calculation of the last step. Also, these errors will add, so the last increment will be influenced by all of the previous errors.

Total strain From the deformation of the entire sample the strains have to be calculated. For this the same manner is used as in DIEKA. In words: for every increment the strain is calculated by adding the strain in the former increment to the strain which is realised in that increment, this is illustrated in Figure 3.10. For the strain in tensile direction, this leads to

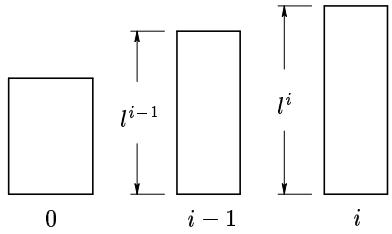

Figure 3.10: The deformed shape

the following definition of the total strain:

$$\varepsilon_y(i) = \frac{l^i - l^{i-1}}{l^{i-1}} + \varepsilon_y(i-1) \tag{3.30}$$

In the limit, where l^i approaches l^{i-1}, this equals the logarithmic strain.

Plastic strain The regular way of determining the plastic strain increment, is to literally use the plastic strain at the beginning and at the end of an increment. This then leads to the following definition of the plastic strain increment:

$$\Delta(\gamma_a^p) = \gamma_a^p(i) - \gamma_a^p(i-1) \tag{3.31}$$

3.6 Conclusion

Recapitulated, in this chapter an algorithm based on the *principle of normality* is introduced to determine the transverse stress σ_x. The algorithm has two principal drawbacks.

The first is that the method elaborates on it's own calculations. The result of the first computation has a large influence on the rest of the sequence. Future research might yield a better method.

The second point of discussion is the required accuracy of the algorithm. Because the calculations are made based on the difference in a deformation step, and not on the absolute value of the quantities, the values will be very small. In Chapter 4 it is investigated if this is the case.

Chapter 4

Simulation results

In this chapter the algorithm is tested by means of simulations in DIEKA. We start with some parameters that are used in the simulations. After that the results of the simulations with and without hardening are presented. In the last part the results are discussed.

4.1 Remarks on the results

In this section an introduction on the simulations is given. Because these simulations can give so much information about strains and stresses, both locally and principally it may be confusing what the determining results are. Therefore a small overview is given.

The most interesting result is whether the calculated transverse stress σ_x corresponds with the results obtained from DIEKA. For the practical evaluation of the algorithm this is done for several strain increment sizes. The simulations performed with DIEKA provide us with the results of all stresses and strains up to nine decimals. In practice these values are not available on this level of accuracy, so it is investigated how accurate the results have to be to supply us with satisfying results.

What also gives an idea of the feasibility of the algorithm is the transformation of the local stresses to principal stresses. An incorrect value of the calculated stress σ_x does not necessarily need to give an incorrect result in the principal stress space.

4.1.1 Size of the deformation increment

As mentioned in Section 3.1 the deformations are divided into two parts, first one step shear, then a number of tensile deformation steps. The first step leads the stress state onto the yield surface, and is defined in such a way that it does only that.

For the actual tests a displacement increment of $2 \cdot 10^{-6}$ mm is chosen for, yet smaller increments do not improve the results. For the situation where a square element of 1x1 mm^2 is used[1], the engineering strain is equal to the displacement increment. The results are improved by using true (logarithmic) strain. For the simulations where hardening is not included a total vertical strain of $3 \cdot 10^{-3}$ is accomplished in 1500 increments. A tensile strain of $9 \cdot 10^{-3}$ for the simulations with hardening is accomplished in 4500 increments.

[1] No other sizes have been used in this thesis

4.1.2 The plane strain singularity

The direction of the plastic strain determines the value of the calculated stress σ_x. As a result, if the direction of the plastic strain is badly defined, the results of σ_x will also be inaccurate. This is the case when the stress state approaches the *plane-strain point*. This is illustrated in Figure 4.1(a)[2]. In Figure 4.1(b) is shown that the *plane-strain point* is not the only point where a singularity occurs. The *shear point* also leads to a plastic deformation which has small components in both the x- and y-direction.

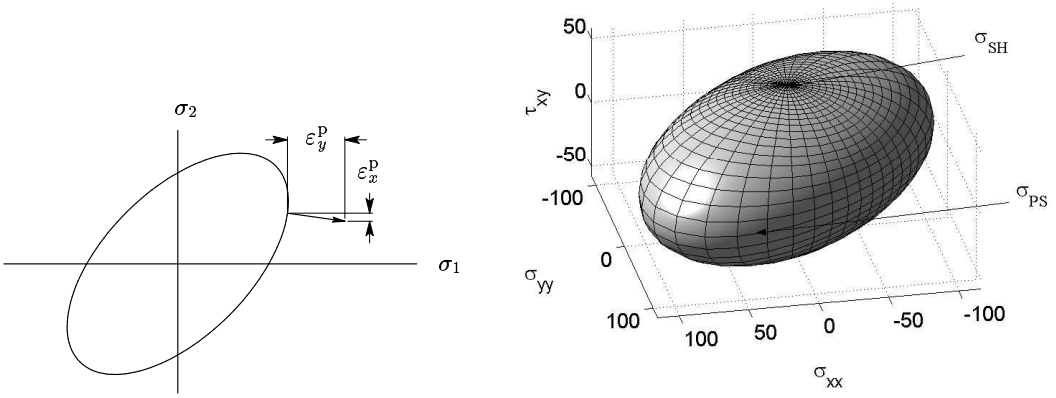

(a) The stress state approaches the *plane-strain point*

(b) 3D representation of the Von Mises yield surface in the local stress space

Figure 4.1: The critical area's for the algorithm

If deformation continues, the algorithm is no longer able to calculate σ_x, because $\Delta\varepsilon_x^{\mathrm{p}}$ approaches zero. This can also be seen in a plot where the plastic strain is depicted, Figure 4.2(b). The plastic strain in x direction ε_x^p reaches a constant level, while the algorithm predicts a decreasing value.

In Figure 4.2 a simulation is performed with 4500 increments and a total tensile strain of $9 \cdot 10^{-3}$. The stress state passes the *uniaxial point* at a strain of approximately $1.2 \cdot 10^{-3}$, the *plane-strain point* is closely approached at the end of the test, $\varepsilon_y = 9 \cdot 10^{-3}$, but will only reach it in the limit. This means that somewhere before the stress state approaches the *plane-strain point*, the simulation has to be stopped.

The deviation in the calculated and in the 'exact' values of the $\varepsilon_x^{\mathrm{p}}$, increases during the test. At the beginning of the test the error increases quickly, up to $\varepsilon_y = 1 \cdot 10^{-3}$ because of the singularity near the *shear point*. After that a stable platform is reached, here the stress state 'rolls' of the sphere. Then the error starts to increase again, at $\varepsilon_y = 5 \cdot 10^{-3}$. After that, the error increases rapidly, due to the singularity at the *plane-strain point*. It is noticed that at the end of the test, the principal stresses hardly change. So the information that is obtained from the last section of the test, does not supply us with much information about the yield locus. With that in mind, the simulation is stopped when the tensile strain has

[2]Because the local stress system is barely rotated compared to the principal system, here the local strains are depicted, and not the strains as a result of the principal stresses

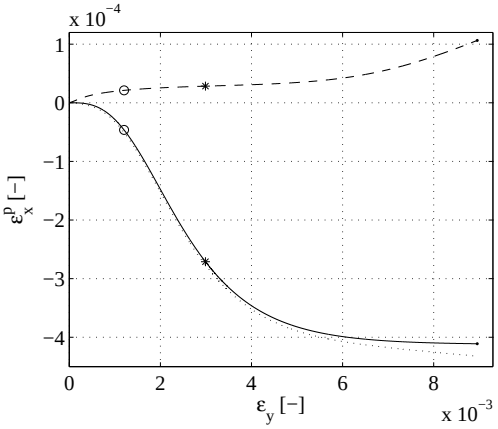

(a) The transverse plastic strain during the test, $\Delta\varepsilon_y = 2 \cdot 10^{-6}$, solid line: 'exact', dotted line: algorithm calculation and the dashed line: deviation(5 X)

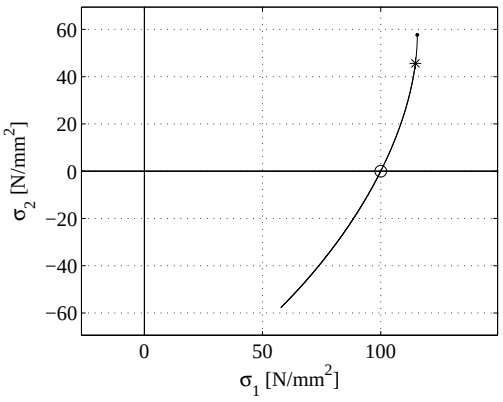

(b) The principal stress space, $\Delta\varepsilon_y = 2 \cdot 10^{-6}$

Figure 4.2: Positions and errors in the calculation: (○): *uniaxial point*, (*): *end of simulation* and (·): *plane-strain point*

reached a value of $\varepsilon_y = 3 \cdot 10^{-3}$. In Figure 4.2 the position in the principals stress space of this strain is depicted with a (*).

It is noticed that the position of the stress state in the principal stress space is dependent on the elastic behaviour and the shape of the yield surface. In this section, the Von Mises criterion is used to determine the amount of tensile strain for a simulation. When the Vegter criterion was used, the numbers would have been a little different. With this in mind, a tensile strain $\varepsilon_y = 1.2 \cdot 10^{-3}$ gives us an indication of the position of the stress state, not a definition. The same holds for the determination of the end of the test. In this thesis however, tests are performed wit a maximum tensile strain of $\varepsilon_y = 3 \cdot 10^{-3}$.

4.1.3 The yield surfaces

For the simulations two yield surfaces are used, The Von Mises criterion and the Vegter criterion. The Von Mises criterion has a relative smooth shape. For the algorithm this should be easy to determine. This is illustrated in Figure 4.3.

Here, the Vegter criterion is defined in such away that a strong curvature exists at the *uniaxial point*. The algorithm probably has more difficulty to follow this shape. This is also the reason why this criterion is used, it may be capable of showing the flaws in the algorithm. The parameters for these yield criteria are shown in Appendix C.

4.2 Ideal plastic behaviour

In this section the algorithm without hardening is tested. First the results from the algorithm are discussed. After that the application window of the algorithm is investigated. In this part

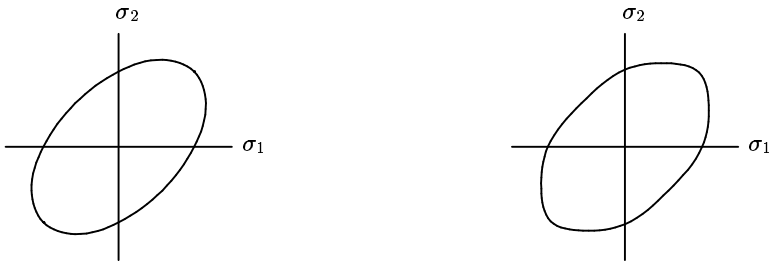

Figure 4.3: On the left-hand side: Von Mises criterion, the right-hand side: Vegter criterion

the deformation is altered during the test and a simulation is performed where a shifted starting point for the modified algorithm is used.

4.2.1 Testing of the algorithm

Here the results from the algorithm, as introduced in Section 3.2 are discussed, applied on two yield surfaces.

The Von Mises criterion

In this section the results from the algorithm applied to the Von Mises criterion are presented. In Figure 4.4 the results are depicted. In Figure 4.4(a) all the planar stresses are depicted, to get a clear picture on the situation during the test. It is noticed that the vertical stress, σ_y, hardly increases at the end of the test, which reflects the ideal plastic behaviour.

In Figure 4.4(c) the calculated stress σ_x is depicted for various tensile strain increments. It is concluded that the stress calculated with the algorithm corresponds better with the 'exact' solution when the strain increments are smaller. The implies a high number of tensile strain increments and readings to calculate the transverse stress properly. At the end of the test, $\varepsilon_y = 3 \cdot 10^{-3}$, the error varies from 1% to 15%. This is obvious because with an increasing strain increment, the stress increment also increases. Hence, the stress increment does not coincide exactly with the yield locus. When the stress increments become smaller, the yield surface is better described with the stress increments.

The principal stresses are depicted in Figure 4.4(b) and in Figure 4.4(d) the details of the area around the *plane-strain point* are depicted. It can be seen that the shape of the yield surface, based on the calculated transverse stress, coincide well with the 'exact' results. Although the transverse stress differs from the 'exact' solution, the shape of the yield locus is well described. The error in the calculation of the transverse stress appears most clearly in the principal stress space around the *plane-strain point*. The stress state is higher than the 'exact' result.

The Vegter criterion

In Figure 4.5 the results from the simulations with the Vegter criterion are depicted. The relatively sharp curve that appears at the *uniaxial point* in the principal stress space also occurs in the local stress space. Especially σ_x demonstrates this phenomenon. It is noticed that the vertical stress, σ_y, hardly increases at the end of the test. This is not only a

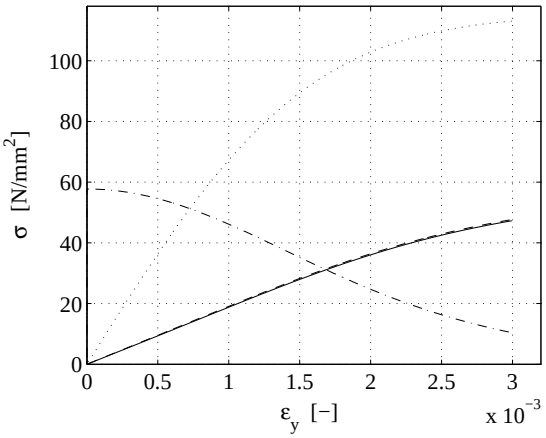

(a) All three local stresses, dotted line: σ_y, dash-dotted line: σ_{xy} and dashed line σ_x with the algorithm, $\Delta\varepsilon_y = 2 \cdot 10^{-6}$

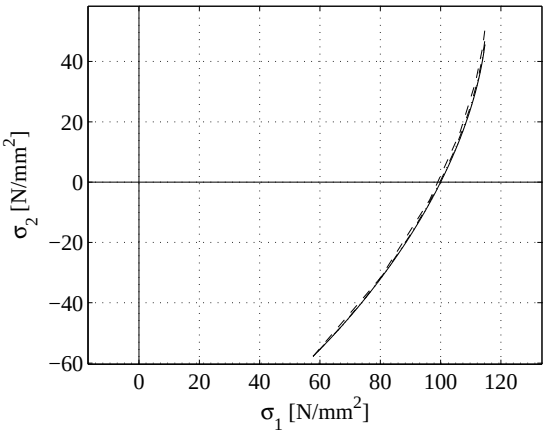

(b) Principal stress space, dotted line: $\Delta\varepsilon_y = 2 \cdot 10^{-6}$, dash-dotted line $\Delta\varepsilon_y = 2 \cdot 10^{-4}$ and dashed line $\Delta\varepsilon_y = 5 \cdot 10^{-4}$

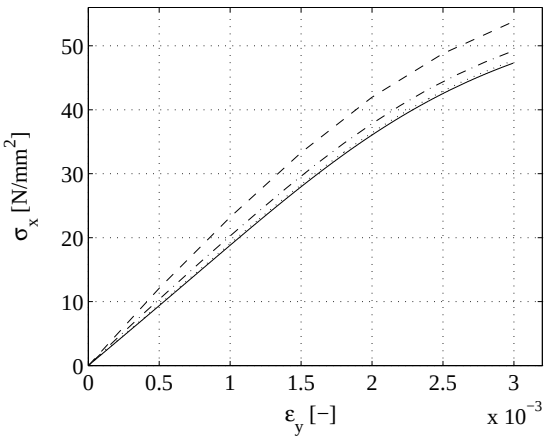

(c) Calculation of σ_x with dashed line: $\Delta\varepsilon_y = 5 \cdot 10^{-4}$, dash-dotted line: $\Delta\varepsilon_y = 2 \cdot 10^{-4}$ and dotted line: $\Delta\varepsilon_y = 2 \cdot 10^{-6}$

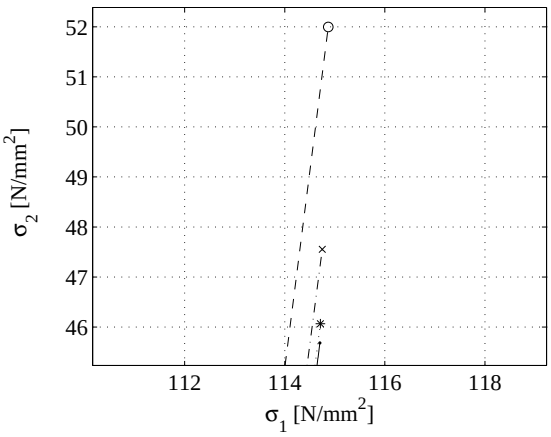

(d) The plane strain area in the principal stress space, dotted line: $\Delta\varepsilon_y = 2 \cdot 10^{-6}$ (*), dash-dot line $\Delta\varepsilon_y = 2 \cdot 10^{-4}$ (x) and dashed line $\Delta\varepsilon_y = 5 \cdot 10^{-4}$ ($\circ$)

Figure 4.4: Calculation of σ_x with the algorithm and with DIEKA (solid line), based on the Von Mises criterion

result of the ideal plastic behaviour, but also the shape of the yield locus contributes to this phenomenon.

In Figure 4.5(c) the transverse stress calculated with the algorithm is depicted. As in the calculations with the Von Mises criterion, the 'exact' stress is better determined when smaller tensile strain increments, $\Delta\varepsilon_y$, are used. It is noticed though that almost no progress is gained when the strain increments are decreased from $2 \cdot 10^{-4}$ to $2 \cdot 10^{-6}$. The calculations of the stress are not as accurate as with the Von Mises criterion. At the end of the test the difference between the calculated and the 'exact' transverse stress varies from 10% to 25%. The error due to the sharp curve in the yield locus result in an addition of 10% compared to the error in the test with the Von Mises criterion.

In the principal stress space, the algorithm follows the yield surface rather good. Again, the simulation with the smaller strain increments show better results than the large strain increments. This is also shown by the large increments in the principal stress space. Especially when the increments leap over the bend at the *uniaxial point*, the surface is more smoothly shaped.

As a conclusion it can be said that the algorithm predicts the stress σ_x rather good. Again the correspondence with the 'exact' solution is better when smaller increments are used. The bend is harder to describe with the algorithm.

Determination of accuracy

In this section the accuracy is discussed. For practical use of the algorithm, an impression of the limits of the capabilities are required. In practise it is not possible to measure a specimen with increments of $2 \cdot 10^{-6}$ mm. The accuracy is not yet available in modern equipment. Also the capability of accurate measurements which provide us with strains up to 9 decimals are not available. Therefore, the algorithm has to be investigated on it's accuracy.
To determine the accuracy two criteria are determined:

- The error in σ_x at a tensile strain of $\varepsilon_y = 3 \cdot 10^{-3}$ may not exceed 20%
- The shape of the calculated curve has to correspond with the shape of the 'exact' result

The first criteria needs some explanation. Because an impression of the capabilities is required, and because an indication for the required measurement equipment is needed, the allowed error is relatively high. When an error of only 1% is allowed, this section would be rather short, only the smallest tensile strain increment and the maximum number of decimals would be appropriate. The second criterion is applied to exclude results that 'accidentally' fall within the error range, but have no further coincidence with the 'exact' result.

The accuracy of the determination of the transverse stress is influenced by two items, errors or flaws from the algorithm itself and errors in the results from the measurements. Only the second item is discussed here; the algorithm can always be improved. The way the algorithm handles errors from the input is discussed here.

When the measurements from the tests are correct, the accuracy is determined by two variables, the size of the strain increments and the numerical accuracy of the measured stresses and strains. With the latter the number of decimals is meant. Not the scientific notation, but the normal notation, *e.g.* with accuracy in 4 decimals 0.0015 and not $1,565 \cdot 10^{-3}$ is meant.

In order to investigate this, two tests are performed. The first starts with increasing the strain increment until one of the criteria does no longer hold. After that the number of

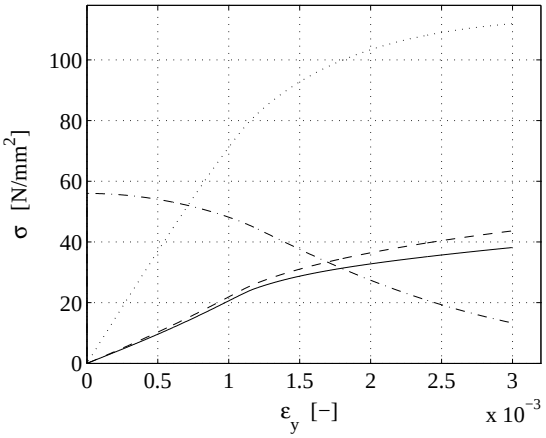

(a) All three local stresses, dotted line: σ_y, dash-dotted line: σ_{xy} and dashed line σ_x with the algorithm, $\Delta\varepsilon_y = 2 \cdot 10^{-6}$

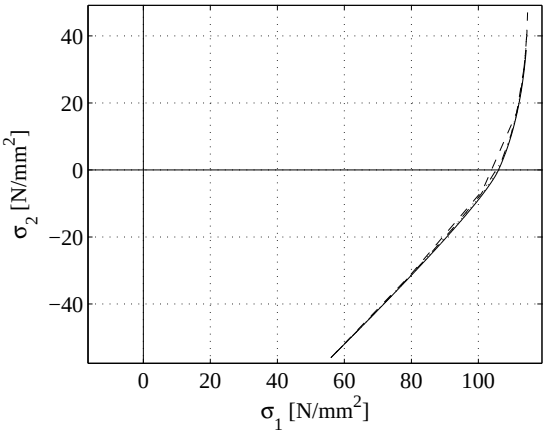

(b) Principal stress space, dotted line: $\Delta\varepsilon_y = 2 \cdot 10^{-6}$, dash-dotted line $\Delta\varepsilon_y = 2 \cdot 10^{-4}$ and dashed line $\Delta\varepsilon_y = 5 \cdot 10^{-4}$

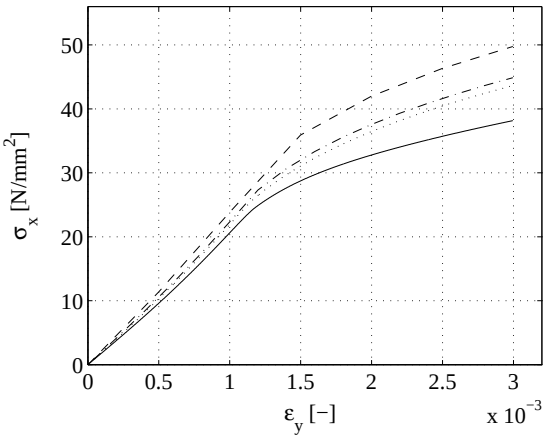

(c) Calculation of σ_x with dashed line: $\Delta\varepsilon_y = 5 \cdot 10^{-4}$, dash-dotted line: $\Delta\varepsilon_y = 2 \cdot 10^{-4}$ and dotted line: $\Delta\varepsilon_y = 2 \cdot 10^{-6}$

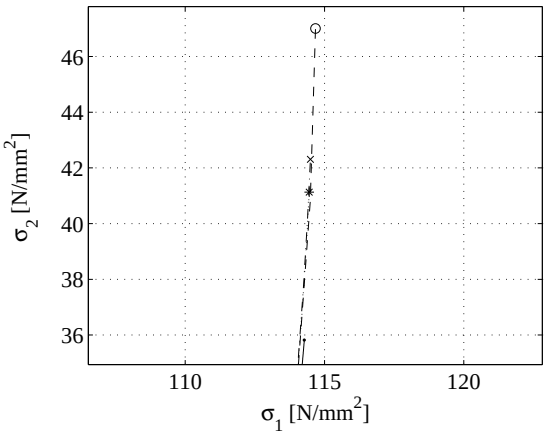

(d) The plane strain area in the principal stress space, dotted line: $\Delta\varepsilon_y = 2 \cdot 10^{-6}$ (*), dash-dot line $\Delta\varepsilon_y = 2 \cdot 10^{-4}$ (x) and dashed line $\Delta\varepsilon_y = 5 \cdot 10^{-4}$ (∘)

Figure 4.5: Calculation of σ_x with the algorithm and with DIEKA (solid line), based on the Vegter criterion

decimals is reduced until one of the criteria no longer holds. The second test is the same as the first, but the sequence is turned around. The test are performed both for the Vegter and the Von Mises criterion.

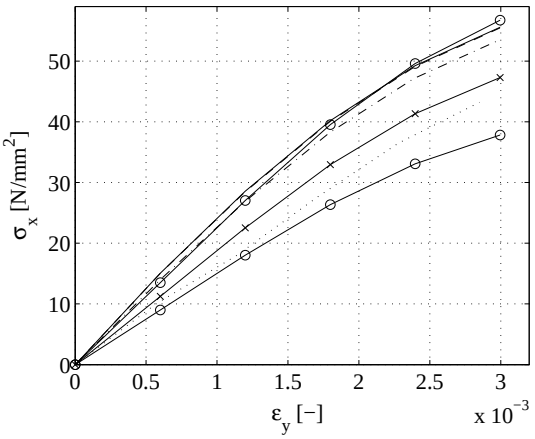

Figure 4.6: Calculation of σ_x with the algorithm with $\Delta\varepsilon_y = 6 \cdot 10^{-4}$, solid line with crosses: exact solution, solid line with circles: boundaries for 20 % error, dotted line: 6 decimals, dash dotted line: 6 decimals, dashed line: 7 decimals and the solid line: 8 decimals

In Figure 4.6 the results of both sequences are depicted. The results are the same, with a tensile strain increment of $6 \cdot 10^{-4}$. The stresses and strains have to be known up to 6 decimals. When larger increments or less decimals are used the results do not satisfy the criteria.

It is noticed that the method of cutting of decimals is done by really 'cutting of' the numbers. The numbers are *not* rounded. As a result the absolute values of the quantities become smaller. If the numbers were rounded the numbers could also be larger. As a result, when the number of decimals decrease, the curve of the transverse stress lowers.

4.2.2 Shifted start and jumps

In this section the possibilities of the algorithm are investigated. This is done with two methods. At first a test where the starting point of the calculations is *not* the *shear point* is discussed. In the second test a jump in the deformation is introduced, this is done by applying extra shear during the test.

A shifted start

In the previous chapter it was discussed that the first point on the yield locus has to be known in order to start the algorithm. Since the material is assumed to behave elastic planar isotropic, the first point can be calculated by using the elastic deformation law, by means of the C-matrix, (2.8). Since the *principle of normality* is not valid in the elastic region, the first step towards the yield surface is determined with the generalised Hookean relation. As a result the stress state has to be 'just' plastic, at the end of the increment.

The first step is now defined as a combination of shear and tensile strain:

$$\Delta\varepsilon_y = 0.0008 \quad , \quad \Delta\gamma_{xy} = 0.0021$$

These values are so defined that the stress state is just on the yield surface, in other words, just a small amount of plastic strain is introduced in this first step. The stress state, in Figure 4.7 reaches the yield locus somewhat higher in comparison with Figure 4.4(b). With this it is demonstrated that the starting point of a measurement does not necessarily has to be the *shear point*.

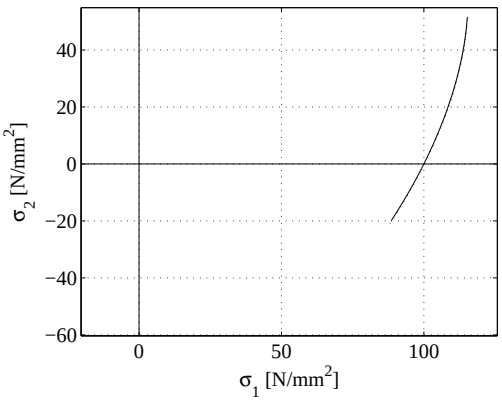

Figure 4.7: The path in the principal stress space for the Von Mises criterion, solid line: exact solution, dashed line: algorithm calculation

In Figure 4.8[3] the local stresses are depicted. At the beginning of the test it can be seen clearly that the shifted starts occur. When the start is at the *shear point*, the local stresses σ_x and σ_y are zero. Because an extra deformation is defined at the start, the stresses σ_x and σ_y directly have a value greater than zero.

The first step is still not very accurate, however hard to see in the figures, but after that the algorithm finds the right track. As in the former simulations, larger increments result in a larger deviation.

Jumps in the deformation path

In this section the result of a jump in the deformation path are discussed. The focus is to investigate if the algorithm is capable of determining the transverse stress with an extra deformation.

The extra deformation that is applied is extra shear. The direction is in accordance with the direction used to get the stress state on the yield surface. When the direction would be opposite, the stress state would enter the elastic region, where the algorithm cannot be used.

The loading path is determined as follows:

1. 1 step shear: $\Delta\gamma_{sh} = 2 \cdot 10^{-3}$

[3]The stresses in this figure are plotted as a function of the number of increments, not the tensile strain, ε_y because in this procedure the tensile strain is a variable.

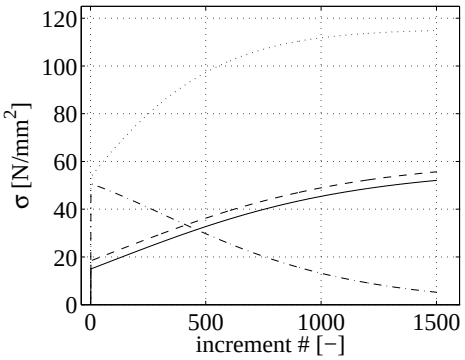

(a) Shifted start for the Von Mises criterion

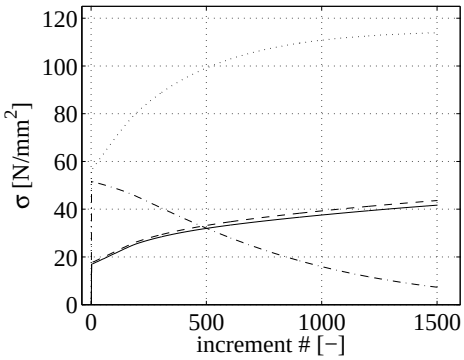

(b) Shifted start for the Vegter criterion

Figure 4.8: All three local stresses, solid line: exact solution for σ_x, dotted line: σ_y, dash-dotted line: σ_{xy} and dashed line σ_x, determined with the algorithm for a shifted starting point,$\Delta\varepsilon_y = 2 \cdot 10^{-6}$

2. 500 steps vertical deformation: $\Delta\varepsilon_y = 2 \cdot 10^{-6}$

3. 1000 steps vertical deformation: $\Delta\varepsilon_y = 2{\cdot}10^{-6}$ and vertical deformation: $\Delta\gamma_{sh} = 3{\cdot}10^{-6}$

This loading path is applied to both the Vegter and the Von Mises criterion. The results are depicted in Figure 4.9. The jumps are best shown by σ_y and σ_{xy}. Particularly the Vegter

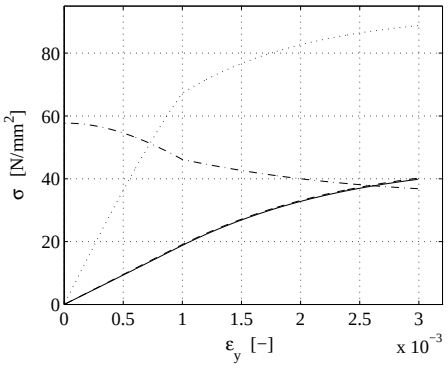

(a) The Von Mises criterion

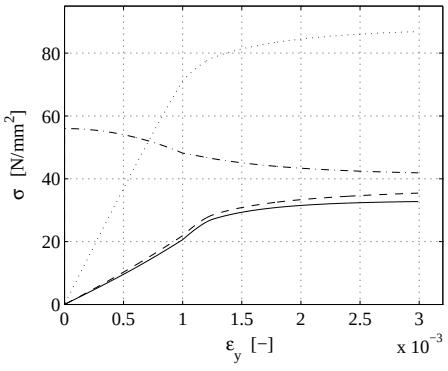

(b) The Vegter criterion

Figure 4.9: All three local stresses, solid line: exact solution forσ_x, dotted line: σ_y, dash-dotted line: σ_{xy} and dashed line σ_x, determined with the algorithm for a deformation path change, $\Delta\varepsilon_y = 5 \cdot 10^{-4}$

criterion shows a sharp bend for σ_y when the shear deformation comes in. The decrease of σ_{xy} becomes smaller when the extra shear is applied. The influence on the transverse stress is minimal.

4.2.3 Discussion

From the simulations it can be concluded that the concept of the algorithm works. As expected, the accuracy of the algorithm is highly dependent on the size of the deformation increments.

The Von Mises criterion is better described by the algorithm than the Vegter criterion. A curvature in the yield locus is harder to describe than a relatively smooth surface and adds an error of approximately 10 %. Also the applications with a shifted start and a jump in the deformation reach the same level of accuracy as the original algorithm.

The test equipment has to be as accurate as possible to gain reliable results. The required accuracy of the strain measurement has to be known up to one thousandth percent. The maximum size of the strain increments are $6{\cdot}10^{-4}$. Another option is to improve the algorithm with an implicit instead of an explicit calculation.

4.3 Simulations with hardening

In this section the results of the simulations without hardening are discussed. Started is with the discussion of the Von Mises criterion, after which the Vegter criterion is discussed. The hardening parameters are discussed in Appendix C. For this moment it is important to know that linear hardening is modelled.

4.3.1 Testing of the algorithm

Here the results from the algorithm with hardening are presented, as discussed in Section 3.3, applied on two yield surfaces.

The Von Mises criterion

In this section the results from the algorithm with hardening applied to the Von Mises criterion are discussed. In Figure 4.10(c) the calculated transverse stress σ_x for various tensile strain increments are depicted is depicted. The shape of the curve is well described by the algorithm, but the tensile strain increment has a large influence on the result. The largest increments, $\Delta\varepsilon_y = 5 \cdot 10^{-4}$ show a deviation of 75%. When the material starts to harden, the absolute difference remains constant.

In Figure 4.10(a) all the planar stress are depicted. From the tensile strain level of $4{\cdot}^{-3}$ the stresses σ_x and σ_y increase with a constant rate. The *plane-strain point* is almost reached and hardening is the dominant factor in the stress increase.

From Figure 4.10(c) it can be concluded that the major part of the error is created during the beginning of the test. After that the deviation is constant. As can be seen in Figure 4.10(d) the equivalent plastic strain slowly increases to a maximum rate. In the first part of the deformation process the angle θ between the local and principal stress system still changes. When the *plane-strain point* is approached, the angle is almost constant and will

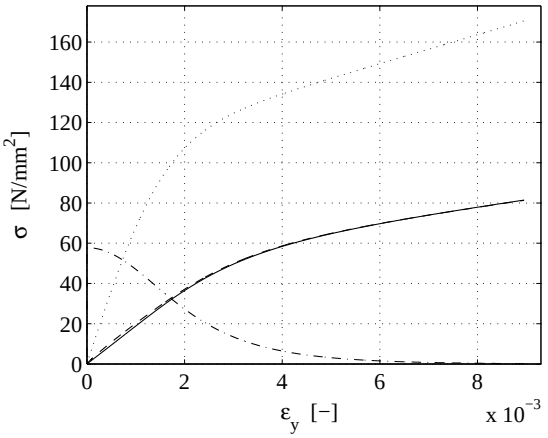

(a) All three local stresses, dotted line: σ_y, dash-dotted line: σ_{xy} and dashed line σ_x with the algorithm, $\Delta\varepsilon_y = 2 \cdot 10^{-6}$

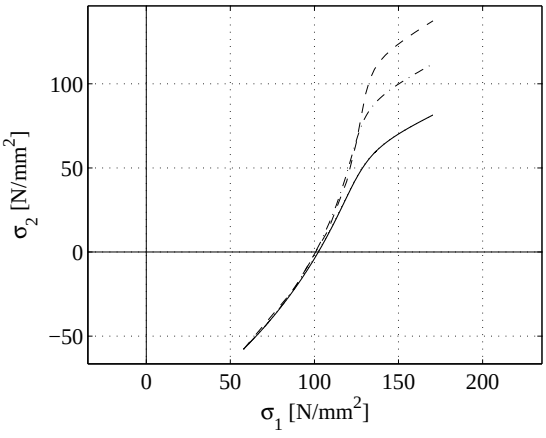

(b) Principal stress space, dotted line: $\Delta\varepsilon_y = 2 \cdot 10^{-6}$, dash-dotted line $\Delta\varepsilon_y = 2 \cdot 10^{-4}$ and dashed line $\Delta\varepsilon_y = 5 \cdot 10^{-4}$

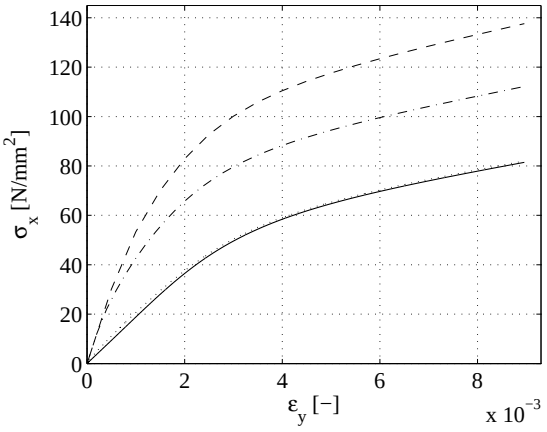

(c) Calculation of σ_x with dashed line: $\Delta\varepsilon_y = 5 \cdot 10^{-4}$, dash-dotted line: $\Delta\varepsilon_y = 2 \cdot 10^{-4}$ and dotted line: $\Delta\varepsilon_y = 2 \cdot 10^{-6}$

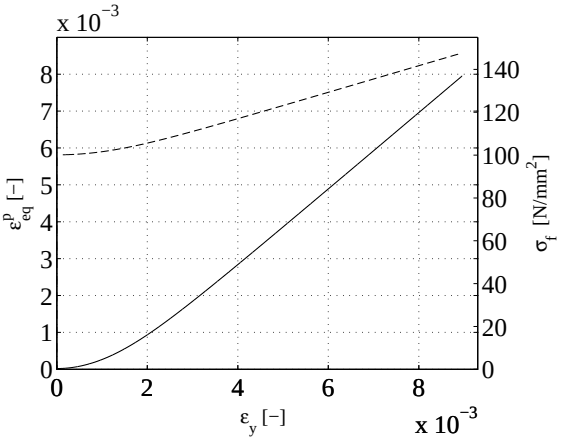

(d) The hardening parameters, solid line: σ_f and the dashed line: ε^p_{eq}

Figure 4.10: Calculation of σ_x with the algorithm for an isotropically hardening material with DIEKA (solid line), based on the Von Mises criterion

just slightly change. This phenomenon may have an effect on the calculation of the hardening during the first part of the deformation.

The Vegter criterion

In this section the results from the algorithm with hardening applied to the Vegter criterion, depicted in Figure 4.12 are discussed. The results are comparable to the results from the Von Mises simulation. Again, the influence of the increment size is huge. Strain increments of $5 \cdot 10^{-4}$ result in an error of almost 100% at a the end of the test, $\varepsilon_y = 9 \cdot 10^{-3}$. The shape of the transverse stress, determined with the algorithm, though, has approximately the same as the shape of the 'exact' solution.

The error is building up during the start of the test. Once the *plane-strain point* is reached, the difference between the 'exact' and the algorithm result remains constant. This is also illustrated by Figure 4.12(b). It can be seen clearly that the hardening is modelled as being linear.

When the tensile strain has reached In Figure 4.12(c) a small irregularity can be seen, when the tensile strain is approximately $1.1 \cdot 10^{-3}$. This is due to the quadratic equation by which the transverse stress is calculated. The quadratic equation discussed in Section 3.4, (3.19), describes a parabola with $\Delta\sigma_x$ as the only variable. It is here denoted with $R = R(\Delta\sigma_x) = 0$. This situation is pictured on the left-hand side of Figure 4.11. The zeros represent the values

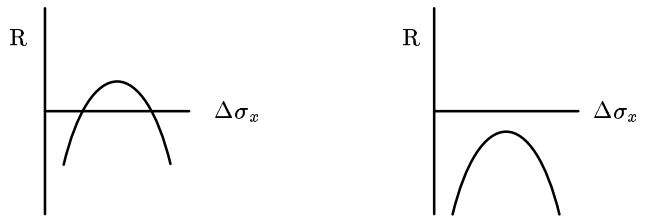

Figure 4.11: The solutions for the transverse stress increment

of $\Delta\sigma_x$ where the plastic strain increment is perpendicular to the yield locus. As the strain increments become smaller, the zeros become closer to one another. A little numerical error can cause a situation where the parabola has no zeros, this is depicted on the right-hand side of Figure 4.11. When this situation occurs there is no $\Delta\sigma_x$ where the *principle of normality* is valid; the plastic strain increment is not perpendicular to the yield surface. For this situation, the top of the parabola is used instead as the value for $\Delta\sigma_x$, as this is the $\Delta\sigma_x$ that approaches the perpendicularity between the plastic strain increment and yield surface the best.

As in the Von Mises simulation the error builds up during the beginning of the test. After that the deviation is roughly constant. This is probably due to the relatively stable situation when the *plane-strain point* is reached.

Accuracy determination

In this section the required accuracy is determined for the algorithm. This item is already discussed in the former section where hardening was excluded. But since the errors in the algorithm without hardening add to the total error for the algorithm with hardening, again the

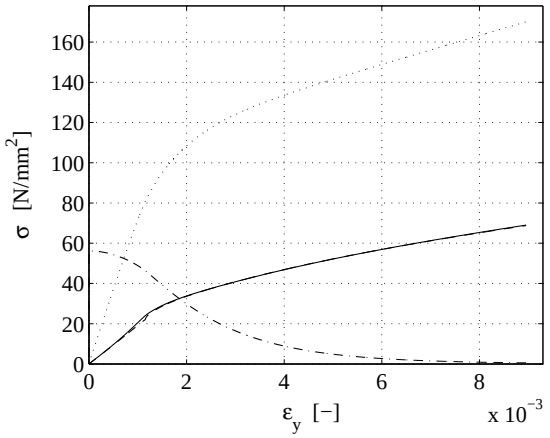

(a) All three local stresses, dotted line: σ_y, dash-dotted line: σ_{xy} and dashed line σ_x with the algorithm, $\Delta\varepsilon_y = 2 \cdot 10^{-6}$

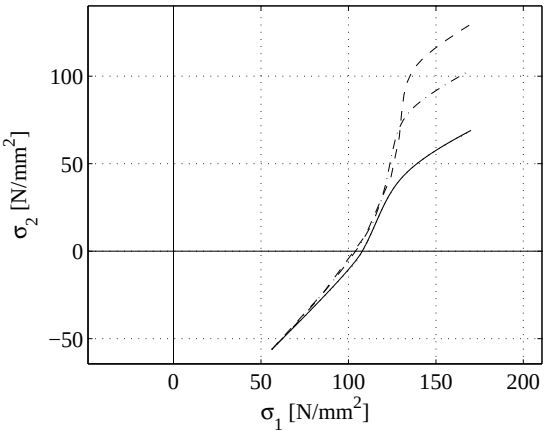

(b) Principal stress space, dotted line: $\Delta\varepsilon_y = 2 \cdot 10^{-6}$, dash-dotted line $\Delta\varepsilon_y = 2 \cdot 10^{-4}$ and dashed line $\Delta\varepsilon_y = 5 \cdot 10^{-4}$

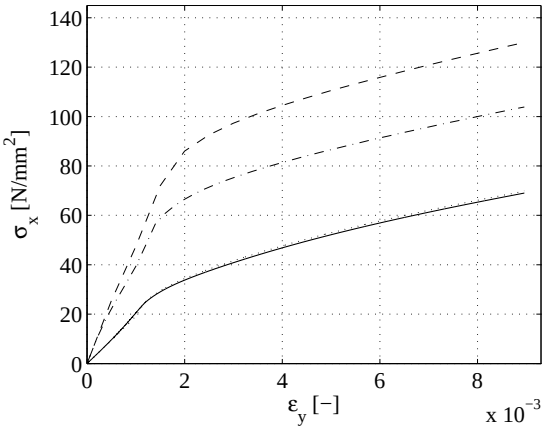

(c) Calculation of σ_x with dashed line: $\Delta\varepsilon_y = 5 \cdot 10^{-4}$, dash-dotted line: $\Delta\varepsilon_y = 2 \cdot 10^{-4}$ and dotted line: $\Delta\varepsilon_y = 2 \cdot 10^{-6}$

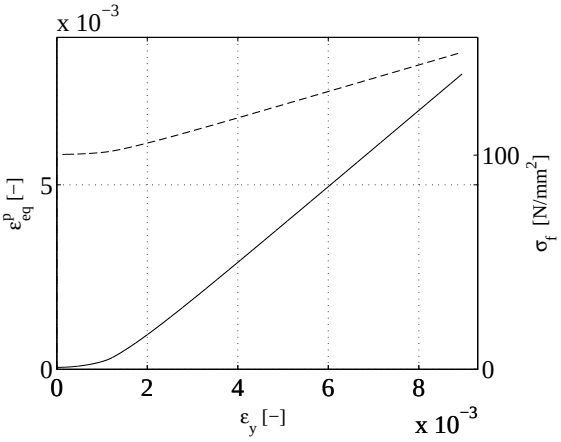

(d) The hardening parameters, solid line: σ_f and the dashed line: ε^p_{eq}

Figure 4.12: Calculation of σ_x with the algorithm for an isotropically hardening material with DIEKA (solid line), based on the Von Mises criterion

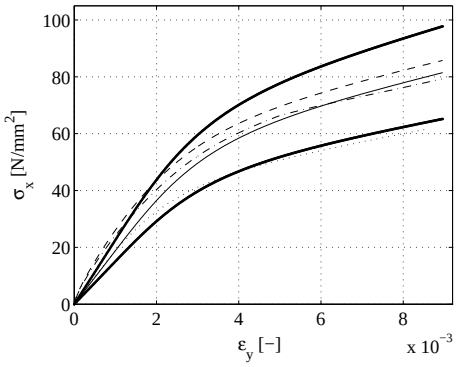

(a) The Von Mises criterion with $\Delta\varepsilon_y = 2 \cdot 10^{-5}$, dotted line: 7 decimals, dash dotted line: 8 decimals and dashed line: 9 decimals

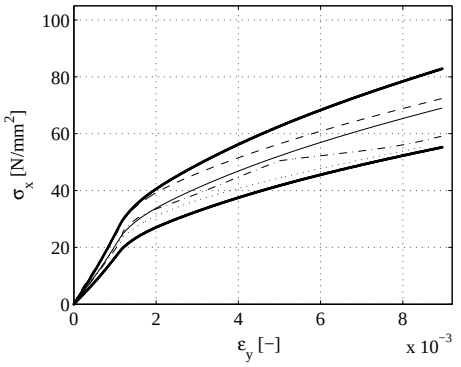

(b) The Vegter criterion with $\Delta\varepsilon_y = 1.2 \cdot 10^{-5}$, dotted line: 7 decimals, dash dotted line: 8 decimals and dashed line: 9 decimals

Figure 4.13: Determination of the transverse stress, solid line: DIEKA-result and the fat lines: 120 % and 80 % of the DIEKA-result for the transverse stress

accuracy is discussed. The method is the same, but now both yield criteria are investigated. In Figure 4.13 the results are depicted.

The criteria used in Section 4.2.1 are also used here; the shape of the curve have to coincide and the maximum error may not exceed 20%. Since the Vegter criteria is harder to describe than the Von Mises criterion, the strain increments have to be are smaller to answer the criteria.

When the results of the two yield criteria are observed, the results show some similarity. When the number of decimals decreases the calculated stress decreases also. But this is the case up to 5 decimals. A further decrease of the numbers of decimals does not have any influence for the calculation of the transverse stress. The curve is more sharp-edged, but the shape still coincides with the result of 7 decimals. This phenomenon is not observed when the algorithm without hardening was discussed. A plausible explanation can not be given for this phenomenon.

4.3.2 Shifted starts and jumps

In this section the application window of the algorithm is investigated. This is done with two methods. As in Section 4.2.2 a test with a shifted starting point and a test with a jump in the deformation path are considered.

Algorithm with shifted start

In this section the algorithm with hardening is tested with a shifted starting point. The first deformation step is the same as in Section 4.2.2.

In Figure 4.14 the results of the local stresses are depicted. For the simulation a strain

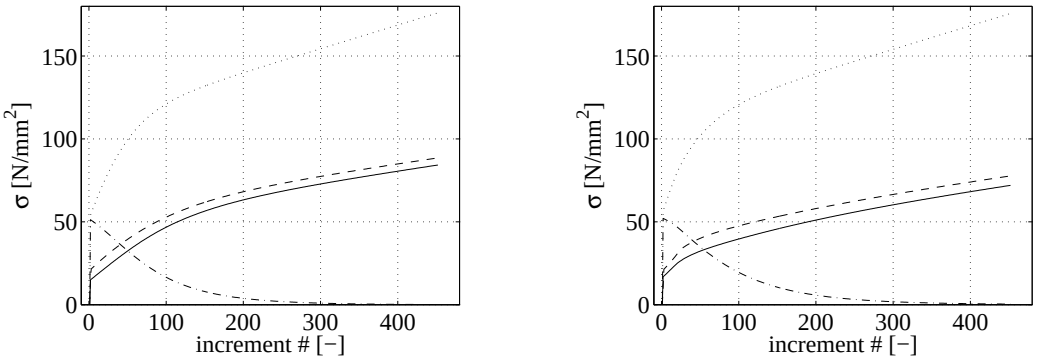

(a) The Von Mises criterion

(b) The Vegter criterion

Figure 4.14: All three local stresses, dotted line: σ_y, dash-dotted line: σ_{xy} and dashed line σ_x, determined with the algorithm for a shifted starting point, with $\Delta\varepsilon_y = 2 \cdot 10^{-5}$

increment of $2 \cdot 10^{-5}$ is used. Again, smaller increments lead to better results, but then the deviation between the results from DIEKA and the algorithm would not be visible.

When the increments are taken small enough, and if the accuracy of the used variables are high enough, the algorithm provides us with reliable information.

Jumps in the deformation path

As in Section 4.2.2, the algorithm is tested when an extra deformation component is added. For this test the deformation is set on the following values

1. 1 step shear: $\Delta\gamma_{sh} = 2 \cdot 10^{-3}$
2. only tensile deformation:$\Delta\varepsilon_y = 1 \cdot 10^{-3}$
3. tensile and shear deformation: $\Delta\varepsilon_y = 8 \cdot 10^{-3}$ and $\Delta\gamma_{sh} = 4 \cdot 10^{-3}$

The results are depicted in Figure 4.15. As in the other simulations, when the increments are enlarged, the error increases. When smaller strain increments are used, the deviation decreases.

When the calculation of the transverse stress is examined, some things draw the attention. For both the simulations, the characteristics of the curves are maintained. Also when the increments are larger, the shape remains the same. The curve for the Von Mises simulation seems quite logical, but for the Vegter simulation an extra bend appears when the shear load is applied, the curve first bends upwards, where after it becomes more horizontal. The algorithm determines these curves quite well. Also visible in Figure 4.15 is the increase of the shear stress when the extra load is applied.

For some extra insight in the deformation and stress paths the principal stresses are depicted in Figure 4.16. In this figure the hardening is well visible, the stress state moves away from the initial yield surface. When this figure is compared to the simulation with

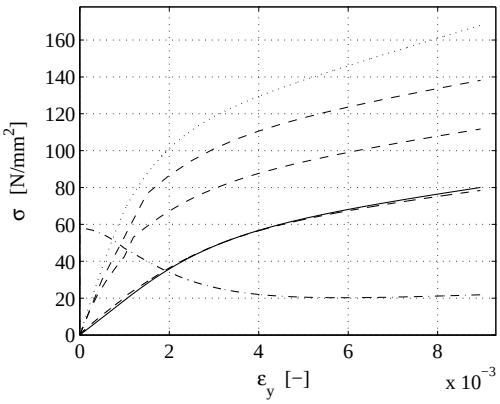

(a) The Von Mises criterion, with dotted line: σ_y and dash-dotted line σ_{sh}

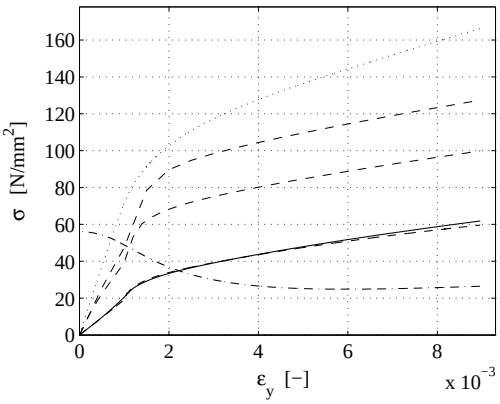

(b) The Vegter criterion, with dotted line: σ_y and dash-dotted line σ_{sh}

Figure 4.15: A jump in the deformation path, with three dashed lines representing σ_x, from top to bottom: $\Delta\varepsilon_y = 5 \cdot 10^{-4}$, $\Delta\varepsilon_y = 2 \cdot 10^{-4}$ and $\Delta\varepsilon_y = 2 \cdot 10^{-6}$, the solid line is the 'exact' solution

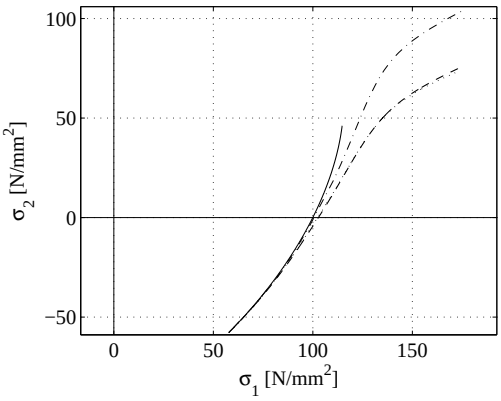

(a) The Von Mises criterion, with dashed line: 'exact' solution, dotted line: $\Delta_y = 2 \cdot 10^{-6}$ and dash-dotted line: $\Delta_y = 2 \cdot 10^{-4}$

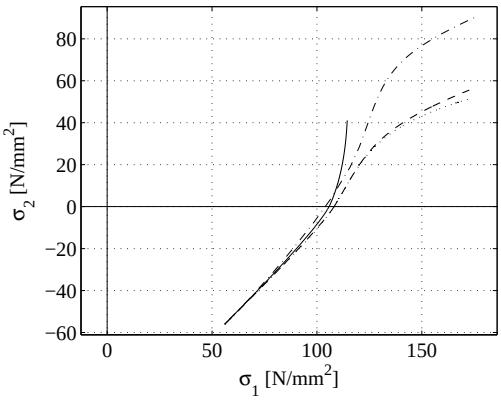

(b) The Vegter criterion, with dashed line: 'exact' solution, dotted line: $\Delta_y = 2 \cdot 10^{-6}$ and dash-dotted line: $\Delta_y = 2 \cdot 10^{-4}$

Figure 4.16: The principal stresses when an extra load is applied in the deformation path, solid line: yield surface without hardening

normal hardening, the curves in Figure 4.16 are 'pushed' away from the initial yield locus by the extra shear load.

4.3.3 Discussion

The discussion in this section does not differ much from Section 4.2.3. The concept of the algorithm is proved and again smaller increments lead to better results. To obtain results that are within the range of 20 % of the 'exact' results the strain has to be known up to one thousandth percent. The maximum size of the strain increment is $1.2 \cdot 10^{-5}$.

The Von Mises criterion is better described with the algorithm than the Vegter criterion. A curve in the yield locus is harder to describe then a relative smooth surface. The applications with a shifted start and a jump in the deformation path supply reliable results.

4.4 Conclusion

In this chapter it is shown that the concept of the algorithm works. Also it is possible to elaborate it with different deformation steps, both at the start or during the tests.

A strongly curved yield locus contributes to an increase of the deviation with approximately 10 %.

The drawback of the algorithm is the required accuracy of the test equipment. Stresses and strains have to be determined with at least six decimals for smooth yield loci, and seven decimals for curved yield loci. The algorithm requires the strain increments to a maximum of $1.2 \cdot 10^{-5}$. Improving the algorithm by means of an implicit calculation instead of an explicit may give better results.

To improve strain measurements two methods are available, strain gauges and an optic laser system. The strain gauges can reach measure the strain, if correctly placed, up to $1 \cdot 10^{-3}$. The disadvantage of this method is that the strain gauges are not manufactured an a size that fits between the two clamps. The available region is 3x20 mm and the limited height is too small for strain gauges. The optic laser system may be a better option. The system measures deformations directly form the surface. The accuracy achieved in deformations with this system is $4 \cdot 10^{-6}$ mm.

Chapter 5

Conclusion and recommendations

5.1 Conclusion

An algorithm is developed to determine the transverse stress in a planar stress situation when only two local stress components are known. The algorithm is based on the *principle of normality*, and uses an incremental method to determine the succession of stress states. The method is developed to be used in experiments with a *biaxial tester*.

From the simulations it is learned that the algorithm is well able to describe planar isotropic behaviour without hardening . The accuracy of the results depends heavily on the size of the tensile strain increments. Smaller tensile strain increments result in a better description of the transverse stress. Tensile strain increments of $2 \cdot 10^{-6}$ give results which are within 1 % of the 'exact' values for a smooth yield surface. A yield surface that is not so smooth, *e.g.* with a bend in it, leads to a deviation of 8 %. If the measured stresses and strain are accurate to 4 decimals and the strain increments are $6 \cdot 10^{-4}$ or smaller, the deviation is less than 20% for a relatively smooth yield surface. Yield surfaces with a stronger curvature in it gives an error up to 30 % with these parameters.

The algorithm is also applied on planar isotropic behaviour with isotropic hardening. Here the accuracy also depends heavily on the size of the strain increments. The deviations though are larger than those found with the algorithm without hardening, because the difference from the algorithm without hardening adds to the error in the algorithm with hardening. Best results are obtained with small strain increments, $2 \cdot 10^{-6}$, both for a smooth and for a curved surface deviation is less then 1 %. Larger strain increments result in larger deviations.

If the measured stresses and strain are accurate to 5 decimals and the strain increments are $2 \cdot 10^{-5}$ or smaller, the deviation is less than 20% for a material with a relatively smooth yield surface and isotropic hardening. For a yield surface that has a bend in it, simulations with 5 decimals and strain increments of $1.2 \cdot 10^{-5}$ result in an error of less then 20 %.

The algorithm is not useful in practise yet. The required accuracy of the stresses and strains are too high for the *biaxial tester*.

5.2 Recommendations

At this point in the development of the algorithm it has no practical use. The algorithm has to be improved to make sense. The accuracy towards the number of decimals has to be increased and also the strain increments have to be enlarged to gain more practical use.

To provide the algorithm with more practical value, it can be expanded with elastic planar anisotropic behaviour. Also the calculation method can be changed from implicit to explicit.

The *biaxial tester* can be upgraded in order to measure more accurately and to prescribe smaller deformations. The determination of the deformation is now done with a camera and four dots applied to the specimen. The deformation can also be traced with a camera and laser setup from *Messphysik* [9], which measures directly from the surfaces. The deformations can be detected with an accuracy of $4 \cdot 10^{-6}$ mm.

In the *biaxial tester* a planar stress situation is created, where one of the three local stresses cannot be directly determined. This phenomenon also exists in the *cruciform test*. Here the two tensile stresses are directly determined and the shear stress is unknown. The algorithm introduced in this thesis can also, with some adjustments, be applied to this test equipment.

Bibliography

[1] Van den Boogaard, A.H. (2002), *Thermally enhanced forming of aluminium sheet*, Ph.D. thesis, University of Twente.

[2] Pijlman, H.H. (2001), *Sheet material characterisation by multi-axial experiments*, Ph.D. thesis, University of Twente.

[3] Vegter, H.P., P. Drent and J. Huétink (1995), A planar isotropic yield criterion based on mechanical testing at multi-axial stress states, in: S.F. Shen and P.R. Dawson (eds.), *Simulation of Materials Processing: Theory, Methods and Applications*, pp 345-350, Balkema, Rotterdam.

[4] Vegter, H. (1991), *On the plastic behaviour of steel during sheet forming*, Ph.D. thesis, University of Twente.

[5] Huétink,J and T. Meinders (2002), *Omvormtechnologie & plasticiteit en kruip*, dictaat (115731), University of Twente.

[6] Drucker, D.C. (1950), *Some Implications of Work-Hardening and Ideal Plasticity*, Quarterly of applied Mathematics, v. 7, n. 4, pp 411-418.

[7] Drucker, D.C. (1952), A more fundamental approach to plastic stress-strain relations, in E. Sternberg (eds.), *Proceedings of the 1st U.S. National Congress of Applied Mechanics*, pp. 487-491, ASME, New York.

[8] Vieira, M.F., J.V. Fernandes and B. Chaparro (2000), Yield stress after double strain-path change, Material Science and Engineering, vol. 284, pp 64-69.

[9] Messphysik materials testing GMBH (2004), *Materials testing*, brochure.

[10] Kuwabara, T., M. Kuroda, V. Tvergaard and K. Nomura (2000), *Use of abrupt strain path change for determining subsequent yield surface: Experimental study with metal sheets*, Acta Materialia, vol 48, pp 2071-2079.

Appendix A

Drucker's postulate

In this appendix Drucker's postulate and the consequences are discussed. Started is with the postulate, after which two results are introduced. The first is the principle of normality, also the yield locus has to be convex, what is discussed in the next section. For this thesis *Drucker's postulate* is given some extra attention, most interesting is the original literature, [6] and [7].

A.1 Drucker's postulate

Though Drucker developed his postulate in an other way, the postulate is best introduced with the uniaxial tensile test. In Figure A.1 the stress strain curve of such a test are depicted. From this curve a stress cycle can be determined, the dash-dotted line represents the start

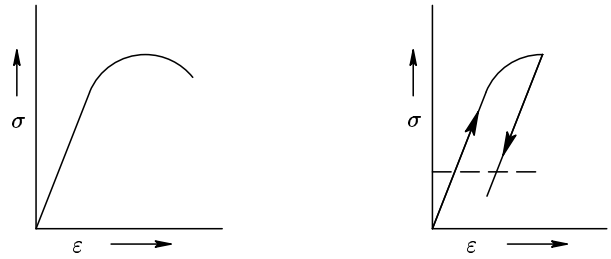

Figure A.1: The stress-strain curve and the stress-cycle

for the stress cycle. The complementary energy is derived as follows

$$W_C = \oint \boldsymbol{\varepsilon} : \mathrm{d}\boldsymbol{\sigma} \tag{A.1}$$

In Figure A.2 the positive energy contribution is denoted with solid lines, and the negative contribution is denoted by the dashed lines. For the instable situation the net result is a positive complementary energy, for the stable situation, the complementary energy is negative. Because energy can not be gained from normal metals in a deformation process, the situation where complementary energy is derived from the deformation process does not exists. This result is encapsulated in *Drucker's postulate*:

$$\oint \boldsymbol{\varepsilon} : \mathrm{d}\boldsymbol{\sigma} \leq 0 \tag{A.2}$$

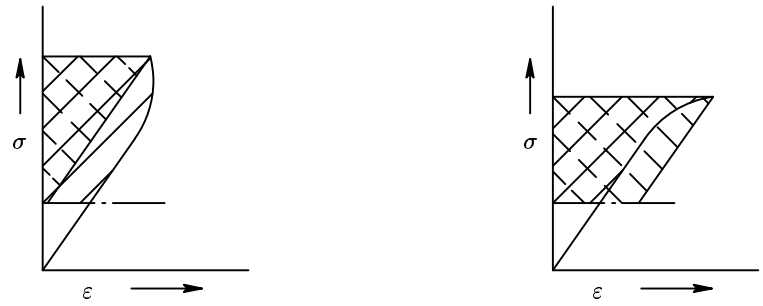

Figure A.2: The stress-strain curve and the stress-cycle

From this postulate the *principle of normality* is derived and it is demonstrated that the yield locus has to be convex.

A.2 Principle of normality

The principle of normality elaborates on *Drucker's postulate*. Started is with a yield locus and a change of stress, see Figure A.3. The stress σ_a denotes the initial stress, σ_v denotes

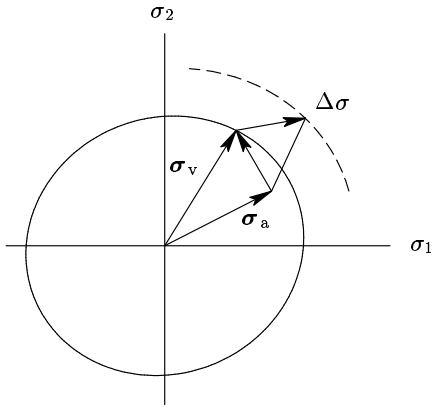

Figure A.3: A change in the stress state

the stress to the yield locus and $\Delta\sigma$ the displacement of the yield locus. The deformation is divided in a elastic and plastic part. The complementary energy becomes:

$$W_C = \oint \boldsymbol{\varepsilon} : \mathrm{d}\boldsymbol{\sigma} = \oint \boldsymbol{\varepsilon}^e : \mathrm{d}\boldsymbol{\sigma} + \oint \boldsymbol{\varepsilon}^p : \mathrm{d}\boldsymbol{\sigma} \tag{A.3}$$

Because elastic deformation is reversible by definition, the former equation is reduced to

$$W_C = \oint \boldsymbol{\varepsilon} : \mathrm{d}\boldsymbol{\sigma} = \oint \boldsymbol{\varepsilon}^p : \mathrm{d}\boldsymbol{\sigma} \tag{A.4}$$

If (A.4) is applied to the cycle in Figure A.3, it follows that

$$\oint \boldsymbol{\varepsilon} : \mathrm{d}\boldsymbol{\sigma} = \oint_{\boldsymbol{\sigma}_\mathrm{v}}^{\boldsymbol{\sigma}_\mathrm{v}+\Delta\boldsymbol{\sigma}} \delta\boldsymbol{\varepsilon}^\mathrm{p} : \mathrm{d}\boldsymbol{\sigma} + \oint_{\boldsymbol{\sigma}_\mathrm{v}+\Delta\boldsymbol{\sigma}}^{\boldsymbol{\sigma}_\mathrm{a}} \Delta\boldsymbol{\varepsilon}^\mathrm{p} : \mathrm{d}\boldsymbol{\sigma} \tag{A.5}$$

The last term represents the elastic spring back. As a result the plastic deformation in this trajectory is constant and so independent of the stress. In the first integral the deformation is dependent on the stress, and is approximated, using the mean value theorem

$$\int_{\boldsymbol{\sigma}_\mathrm{v}}^{\boldsymbol{\sigma}_\mathrm{v}+\Delta\boldsymbol{\sigma}} \delta\boldsymbol{\varepsilon}^\mathrm{p} : \mathrm{d}\boldsymbol{\sigma} = \alpha\Delta\boldsymbol{\varepsilon}^\mathrm{p} : \Delta\boldsymbol{\sigma} \tag{A.6}$$

This is applied to (A.5)

$$\oint \boldsymbol{\varepsilon} : \mathrm{d}\boldsymbol{\sigma} = \alpha\Delta\boldsymbol{\varepsilon}^\mathrm{p} : \Delta\boldsymbol{\sigma} + \Delta\boldsymbol{\varepsilon}^\mathrm{p} : (\boldsymbol{\sigma}_\mathrm{a} - \boldsymbol{\sigma}_\mathrm{v} - \Delta\boldsymbol{\sigma}) \tag{A.7}$$

In the limit the plastic deformation approaches 0, so the terms $O(\Delta^2)$ are neglected. This leads to

$$\oint \boldsymbol{\varepsilon} : \mathrm{d}\boldsymbol{\sigma} = \mathrm{d}\boldsymbol{\varepsilon}^\mathrm{p} : (\boldsymbol{\sigma}_\mathrm{a} - \boldsymbol{\sigma}_\mathrm{v}) \tag{A.8}$$

According to *Drucker's postulate*, the right-hand side of (A.8) is equal or smaller than 0

$$(\boldsymbol{\sigma}_\mathrm{v} - \boldsymbol{\sigma}_\mathrm{a}) : \mathrm{d}\boldsymbol{\varepsilon}^\mathrm{p} \geq 0 \tag{A.9}$$

If (A.9) is considered with the example of Figure A.3, it is shown that the 'vectors' $(\boldsymbol{\sigma}_\mathrm{v} - \boldsymbol{\sigma}_\mathrm{a})$ and $\mathrm{d}\boldsymbol{\varepsilon}^\mathrm{p}$ make a sharp angle, or are perpendicular to each other (inproduct ≥ 0). This is depicted in Figure A.4 where two different initial situations, $\boldsymbol{\sigma}_\mathrm{a}$ and $\boldsymbol{\sigma}_\mathrm{a}^*$, are depicted. A

Figure A.4: Two different stress states

plastic deformation increment belonging to $\boldsymbol{\sigma}_\mathrm{v}$ needs to be positioned in the hatched areas. When both vectors $\boldsymbol{\sigma}_\mathrm{a}$ and $\boldsymbol{\sigma}_\mathrm{a}^*$ in the limit approach $\boldsymbol{\sigma}_\mathrm{v}$, the vector $\mathrm{d}\boldsymbol{\varepsilon}^\mathrm{p}$ is enclosed by the two boundaries, this is depicted in Figure A.5. When the yield locus is smooth, the plastic deformation increment is perpendicular to the yield locus. This is known as the *principle of normality.*

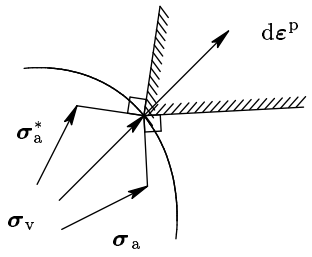

Figure A.5: The plastic strain increment is perpendicular to the yield locus

A.3 Convexity of the yield locus

From the *principle of normality* it is reasoned that the yield locus has to be convex.

In the imaginary situation that the plastic strain increment has an angle greater than 90°, Equation (A.9) is no longer valid. This would lead to a situation where energy is gained from plastic deformation.

An angle greater than 90° is possible when the yield surface is concave. This is depicted in Figure A.6. As a result the yield surface has to be convex.

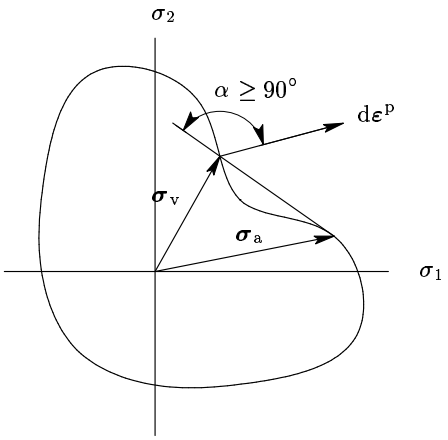

Figure A.6: The yield locus has to be convex

Appendix B

Other tests

In this section the methods are described which are generally used to acquire useful parameters from the material. The tests discussed here are concerned with sheet metal. Each test defines a specific point on the yield locus, this is shown in Figure B. These points are; shear test (SH), uniaxial test(UN), plane-strain test(PS) and the equi-biaxial test(BI). In the following

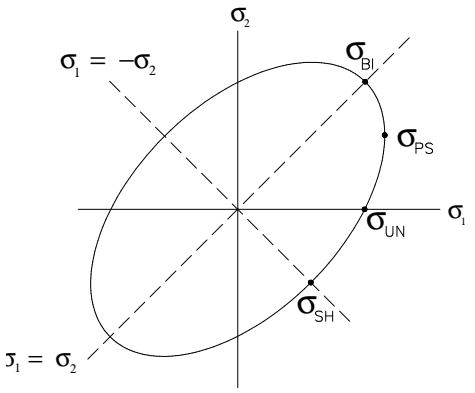

Figure B.1: The four regular points to describe a yield locus

paragraphs these tests will shortly be discussed.

B.1 Tensile test

The conventional uni-axial test defines the location and the gradient of the uniaxial reference point. A regular test specimen is drawn in Figure B.1 The gradient can be determined from the strains in the normal and transverse direction. This is done by means of the total differential equation:

$$\phi = \phi(\sigma_x, \sigma_z) \quad \Longleftrightarrow \quad \mathrm{d}\phi = \left(\frac{\partial \phi}{\partial \sigma_x}\right) \mathrm{d}\sigma_x + \left(\frac{\partial \phi}{\partial \sigma_z}\right) \mathrm{d}\sigma_z \tag{B.1}$$

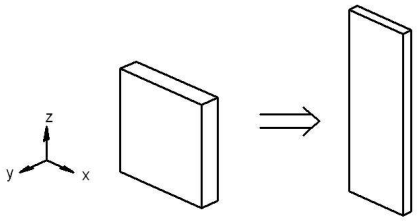

Figure B.2: A normal test specimen for a tensile test.

When the specimen is loaded to the yield surface, the yield surface won't change shape and so equation B.1 has to equal zero:

$$\mathrm{d}\phi = 0 = \left(\frac{\partial \phi}{\partial \sigma_x}\right)\mathrm{d}\sigma_x + \left(\frac{\partial \phi}{\partial \sigma_z}\right)\mathrm{d}\sigma_z \quad \Longleftrightarrow x \quad \frac{\mathrm{d}\sigma_x}{\mathrm{d}\sigma_z} = -\frac{\frac{\partial \phi}{\partial \sigma_z}}{\frac{\partial \phi}{\partial \sigma_x}} \tag{B.2}$$

Because the plastic deformation is perpendicular to the yield surface, the fractions of the stresses gives the gradient of the yield surface:

$$-\frac{\frac{\partial \phi}{\partial \sigma_z}}{\frac{\partial \phi}{\partial \sigma_x}} = -\frac{\mathrm{d}\varepsilon_z}{\mathrm{d}\varepsilon_x} = -\frac{-\mathrm{d}\varepsilon_y - \mathrm{d}\varepsilon_x}{\mathrm{d}\varepsilon_x} = \frac{1+R}{R} \tag{B.3}$$

B.2 Simple shear test

This test defines the location and the gradient of the shear point on the yield surface. A pure shear test consists of two perpendicular loads but pointed opposite. Such an experiment is difficult because it's hard to keep both loads equal. Therefore the shear test is performed by clamping the test specimen on two sides and shift one clamp in transverse direction, see also Figure B.2. This test is called the simple shear test.

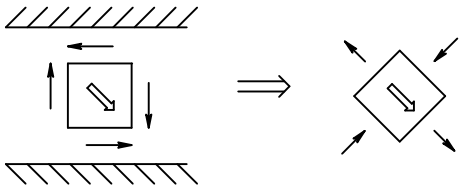

Figure B.3: The simple shear test

B.3 Cruciform test

The cruciform test is performed on a squared piece of sheet material which can be loaded in two perpendicular directions. Most commonly it is used to determine the equi-bi-axial point. A test specimen is depicted in Figure B.3. Although the cruciform test seems to be a good tool to determine the *equi-bi-axial point*, in practice it is difficult to keep both stresses exactly the same. Therefore the *equi-bi-axial point* can be determined by means of a compress test. This

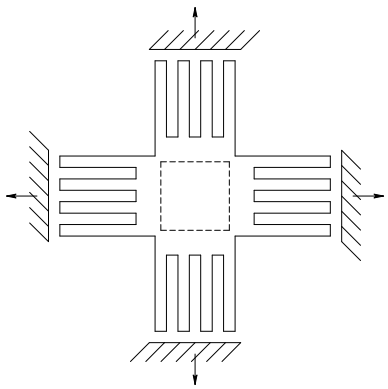

Figure B.4: A cruciform test specimen

is possible when is assumed that the material behaviour is independent of the hydrostatic pressure. The gradient is determined by the normality principle, the ratio of the in plane strains. Although the cruciform test is hard to handle in practice, it still is an interesting

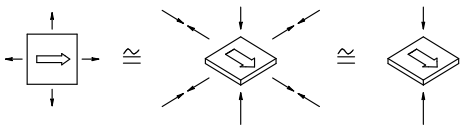

Figure B.5: The cruciform test is equivalent to the hydrostatic test

piece of test equipment. Because two loads can be applied mutually independent, a whole range of stress situation can be realised. From this it may be possible to determine a piece of the yield surface, instead of just one point.

Appendix C

Simulation data

In this appendix, the characteristic values for the simulations are presented. Data are needed to describe the yield loci for both the Von Mises and the Vegter criterion. The material is assumed to be planar isotropic. The elastic region is determined as in Table C.1.

E	$7 \cdot 10^4$ N/mm^2
ν	0.25 [−]

Table C.1: Characterisation of the elastic region

The yield stress as used in the both criteria is 100 N/mm^2. By means of the flow stress the Von Mises criterion is fixed. The Vegter criterion is further determined with the data from Table C.2

f_{bi}	1.02
f_{ps}	1.15
f_{un}	1.06
f_{sh}	0.56
α_{ps}	0.5
R-value	0.85
$\dot{\varepsilon}_2/\dot{\varepsilon}_1$	1.0

Table C.2: Characterisation of vegter yield locus

The hardening parameters are obtained from an uniaxial test, for this thesis the hardening is defined as follows:

$$\begin{aligned} \sigma_{\text{f}} &= \sigma_0 + h\,\varepsilon_{\text{eq}}^{\text{p}} \qquad \text{, with} \\ h &= 6000 \text{ N/mm}^2 \\ \sigma_0 &= 100 \text{ N/mm}^2 \end{aligned} \tag{C.1}$$

These parameters are used in the simulations with isotropically hardening.